Available online at www.sciencedirect.com
ScienceDirect
Geochimica et Cosmochimica Acta 71 (2007) 5072–5088
Geochimica et Cosmochimica Acta
www.elsevier.com/locate/gca

Oxygen isotope partitioning during oxidation of pyrite by H_2O_2 and its dependence on temperature

Liliana Lefticariu [a,c,*], Arndt Schimmelmann [b], Lisa M. Pratt [b,c], Edward M. Ripley [b,c]

[a] Department of Geology, Southern Illinois University, Carbondale, IL, USA
[b] Department of Geological Sciences, Indiana University, Bloomington, IN, USA
[c] Indiana Princeton Tennessee Astrobiology Initiative (IPTAI), NASA Astrobiology Institute, Indiana University, Bloomington, IN, USA

Received 23 February 2007; accepted in revised form 20 August 2007; available online 19 September 2007

Abstract

A detailed experimental study was conducted to investigate mechanisms of pyrite oxidation by determining product yields and oxygen isotopic fractionation during reactions between powdered pyrite (FeS_2) with aqueous hydrogen peroxide (H_2O_2). Sealed silica-tube experiments utilized aliquots of pyrite that were reacted with 0.2 M H_2O_2 for 7 to 14 days at 4 to 150 °C. No volatile sulfur species were detected in any experiment. The only gaseous product recovered was elemental oxygen inferred to result from decomposition of H_2O_2. Aqueous sulfate (S_{aq}) was the only sulfur product recovered from solution. Solid hydrated ferric iron sulfates (i.e., water-soluble sulfate fraction, S_{ws}) were recovered from all experiments. Ferric oxide (hematite) was detected only in high temperature experiments.

Reactants were selected with large differences in initial $\delta^{18}O$ values. The oxygen isotopic compositions of oxygen-bearing reactants and products were analyzed for each experiment. Subsequent isotopic mass-balances were used to identify sources of oxygen for reaction products and to implicate specific chemical reaction mechanisms. $\delta^{18}O$ of water did not show detectable change during any experiment. $\delta^{18}O$ of sulfate was similar for S_{aq} and S_{ws} and indicated that both H_2O and H_2O_2 were sources of oxygen in sulfate. Low-temperature experiments suggest that H_2O-derived oxygen was incorporated into sulfate via Fe^{3+} oxidation, whereas H_2O_2-derived oxygen was incorporated into sulfate via oxidation by hydroxyl radicals ($HO^{\cdot}$). These two competing mechanisms for oxygen incorporation into sulfate express comparable influences at 25 °C. With increasing reaction temperatures from 4 to 100 °C, it appears that accelerated thermal decomposition and diminished residence time of H_2O_2 limit the oxygen transfer from H_2O_2 into sulfate and enhance the relative importance of H_2O-derived oxygen for incorporation into sulfate. Notably, at temperatures between 100 and 150 °C there is a reversal in the lower temperature trend resulting in dominance of H_2O_2-derived oxygen over H_2O-derived oxygen. At such high temperatures, complete thermal decomposition of H_2O_2 to water and molecular oxygen (O_2) occurs within minutes in mineral-blank experiments and suggests little possibility for direct oxidation of pyrite by H_2O_2 above 100 °C. We hypothesize that a $Fe–O_2$ mechanism is responsible for oxygenating pyrite to sulfate using O_2 from the preceding thermal decomposition of H_2O_2.

1. INTRODUCTION

Oxidation of sulfide minerals in the presence of water and oxygen (O_2) near the surface of Earth frequently results in production of highly acidic, sulfate-rich solutions associated with weathering of metalliferous black shales, coal beds, and metal-sulfide ores. During the past two decades numerous studies have concentrated on understanding the mechanism of pyrite oxidation (Lowson, 1982; McKibben and Barnes, 1986; Luther, 1987; Moses et al., 1987; Williamson and Rimstidt, 1994; Evangelou, 1995; Rimstidt and Vaughan, 2003), due in part to the environmental

* Corresponding author. Fax: +1 618 453 7393.
E-mail address: Lefticariu@geo.siu.edu (L. Lefticariu).

0016-7037/$ - see front matter © 2007 Elsevier Ltd. All rights reserved.
doi:10.1016/j.gca.2007.08.022

impact of acid mine drainage (Singer and Stumm, 1970; Alpers and Blowes, 1994; Evangelou and Zhang, 1995; Seal and Wandless, 1997; Banks et al., 1997; Jambor et al., 2003; Nordstrom et al., 2000).

At depths greater than a few tens of meters below Earth's surface, aqueous fluids are often anoxic due to rapid utilization of oxygen and other electron acceptors by microbes in soil, sediment, and groundwater. In spite of presumed widespread anoxia, there is evidence of subsurface oxidation during the genesis of uranium roll-front deposits and the alteration of sulfide-bearing ores and coals (Vovk, 1982; Dubessy et al., 1988; Vovk, 1987; Liu et al., 1996; Savary and Pagel, 1997; Fayek et al., 1997). Traditionally O_2 and H_2O have been viewed as the sources of oxygen for production of sulfate from metal-sulfide ore deposits (Mizutani and Rafter, 1973; Taylor et al., 1984a; Toran and Harris, 1989; Krouse et al., 1991; Rye et al., 1992; Taylor and Wheeler, 1994). Radiolysis of water in the presence of uranium-bearing ore bodies may also provide highly oxidizing, reactive oxygen species (Vovk, 1987; Savary and Pagel, 1997; Burns and Hughes, 2003; Amme et al., 2005; Lin et al., 2005; Lin et al., 2006). Radiolytic cleavage of water molecules as a result of alpha-, beta-, and gamma-radiation can produce a mixture of strong oxidants, including hydrogen peroxide (H_2O_2) and hydroxyl radicals ($HO^{\bullet}$) if the initial metastable products of radiolysis do not rapidly recombine to form water molecules (Allen, 1961; Buxton, 1987; Spinks and Woods, 1990; Garrett et al., 2004). Radiation-induced chemical reactions resulting in oxidation are particularly significant in geologic environments where the fugacity of molecular oxygen is negligible (Warren, 1972; Vovk, 1987; Lin et al., 2005; Lin et al., 2006). The long-time geochemical effects of water radiolysis are important for both fundamental and practical reasons, and yet, almost no basic experimental studies have been performed to evaluate the interaction of radiolytically produced oxidants with sulfides. This constitutes a major limitation to our understanding of oxidative processes in Earth's lithosphere and in the interior of other planetary bodies with significant inventories of radioactive nuclides.

Recently, much interest has focused on sulfide oxidation due to the discovery of sulfate minerals on Mars and the similarity of Martian mineral assemblages with minerals associated with acid drainage on Earth (Baird et al., 1976; Christensen et al., 2004; Squyres et al., 2004; Gendrin et al., 2005; Bibring et al., 2005; McLennan et al., 2005). Furthermore, the intrinsic association of sulfate minerals with liquid water is consistent with surface or near-surface water being present during Martian history (Bishop and Murad, 1996; Vaniman et al., 2004; Clark et al., 2005; Elwood Madden et al., 2004). Sulfate-solutions host diverse microbial communities on the surface and in the subsurface of Earth, lending credence to the search for evidence of extinct or extant life on Mars (Knoll et al., 2005; Grotzinger et al., 2005; Schulze-Makuch and Irwin, 2006; Atreya et al., 2006). The chemical and isotopic compositions of Martian sulfate minerals bear valuable clues about past and recent geochemical processes and can help our understanding of the history of water and the potential presence of life on Mars.

This contribution presents the first stable isotope data relating to oxygen isotopic partitioning in a system containing H_2O, pyrite, and H_2O_2. We used H_2O_2 as an analog for radiolytically produced oxidants, since H_2O_2 rather than O_2 is the main oxidizing species produced during radiolysis of water (Allen, 1961; Buxton, 1987; Pastina and LaVerne, 2001; Garrett et al., 2004). Our previous contribution (Lefticariu et al., 2006) demonstrated that sulfur isotopic fractionations provided minimal constraints on chemical mechanisms of pyrite oxidation by H_2O_2. Surprisingly, our results from ^{18}O-labeled experiments show a complicated dependence of oxygen isotopic composition of sulfate ($\delta^{18}O_{SO_4}$) on temperature of reaction, suggesting competing oxidation mechanisms for pyrite at different temperatures. Distinct oxygen isotopic signatures for produced sulfate are related to different pathways of oxygen incorporation from H_2O_2 and H_2O. Additional experimental work is required to further resolve potential mechanisms of radiolytic oxidation of pyrite and to extend analytical studies into natural environments.

2. BACKGROUND

Oxidation of pyrite to sulfate at low temperatures in contact with an aqueous phase is commonly described by two end member reactions (Lowson, 1982; McKibben and Barnes, 1986; Luther, 1987; Rosso et al., 1999; Kamei and Ohmoto, 1999; Rimstidt and Vaughan, 2003; Borda et al., 2004) that differ in (i) oxidizing agent, the activities of ferric iron and/or dissolved oxygen (reactions (R1) and (R2), respectively), and (ii) inferred sources of oxygen (O_2 and/or H_2O) for the formation of sulfate. Ferric iron (Fe^{3+}) is a powerful oxidant of pyrite in highly acidic conditions (Garrels and Thompson, 1960; Singer and Stumm, 1970; Moses et al., 1987; Nordstrom and Alpers, 1999), and reacts with pyrite according to the following reaction:

$$FeS_2 + 14Fe^{3+} + 8H_2O \rightarrow 15Fe^{2+} + 2SO_4^{2-} + 16H^+ \quad (R1)$$

Aqueous pyrite oxidation by O_2 is represented by the following overall reactions:

$$FeS_2 + 3.5O_2 + H_2O \rightarrow Fe^{2+} + 2SO_4^{2-} + 2H^+ \quad (R2)$$

Ferrous iron (Fe^{2+}) is released into solution where it is oxidized to ferric iron:

$$4Fe^{2+} + O_2 + 4H^+ \rightarrow 4Fe^{3+} + 2H_2O \quad (R3)$$

The mechanism of pyrite oxidation by H_2O_2 is unknown. Nevertheless, pyrite oxidation by hydrogen peroxide may be represented by the following generalized reaction:

$$2FeS_2 + 15H_2O_2 \rightarrow 2Fe^{3+} + 4SO_4^{2-} + 14H_2O + 2H^+ \quad (R4)$$

Rimstidt and Vaughan (2003) presented an electrochemical model of pyrite oxidation describing concurrent anodic and cathodic reactions. The cathodic reaction involves aqueous species accepting electrons from Fe^{2+} sites on mineral surfaces. Anodic reactions represent the stepwise abstraction of 7 sulfur electrons from the sulfidic S(−I)

state in pyrite FeS_2 ultimately leading to the S(VI) state in sulfate. According to this model, the role of the oxidant (Fe^{3+} or O_2) is simply to accept and carry away electrons that are released by the Fe^{2+} sites on pyrite surfaces, as the sulfur oxidizes and interacts with oxygen from H_2O molecules to become sulfate (Rimstidt and Vaughan, 2003). Thus, regardless of the oxidant, Fe^{3+} or O_2, the oxygen incorporated into the product sulfate comes exclusively from H_2O. When O_2 is the oxidant, it probably interacts with Fe^{2+} sites on the pyrite surface (reaction (R3)), but not directly with sulfur atoms (Lowson, 1982; Rosso et al., 1999; Rimstidt and Vaughan, 2003).

Experimental studies have shown that during oxidation of pyrite by Fe^{3+} (reaction (R1)), water is the only source of oxygen in sulfate (Reedy et al., 1991), in agreement with the electrochemical model. However, experimental data have shown that during aqueous pyrite oxidation by O_2, some O_2-derived oxygen is incorporated into sulfate (Taylor et al., 1984b; Reedy et al., 1991; Usher et al., 2005). In addition, compilations of field data have shown that $\delta^{18}O_{SO_4}$ in mine-drainage often differs from that of the associated water $\delta^{18}O_{H_2O}$ (Toran and Harris, 1989; Taylor and Wheeler, 1994; van Stempvoort and Krouse, 1994; Seal, 2003), suggesting that O_2 is incorporated into sulfate. Two mechanisms have been invoked to explain these data. First, bacterial processes (e.g., van Everdingen and Krouse, 1985; van Stempvoort and Krouse, 1994) can strongly influence the pathways for O_2 incorporation into sulfate and thus influence the oxygen isotope signature of the resulting sulfate (Edwards et al., 2000; Böttcher et al., 2001; Canfield, 2001; Aharon and Fu, 2003). Second, Lloyd (1967, 1968) demonstrated that the incorporation of O_2 into intermediate sulfoxyanions is possible in solution during the oxidation of sulfite SO_3^{2-} to sulfate SO_4^{2-}, according to the reaction:

$$SO_3^{2-} + 1/2O_2 \rightarrow SO_4^{2-} \quad (R5)$$

At high pH > 6, intermediate sulfoxyanion species, such as polythionates, thiosulfates, and sulfite, have been identified in sulfide-mineral oxidation experiments (Goldhaber, 1983; McKibben and Barnes, 1986; Moses et al., 1987). Dissolved intermediate sulfoxyanions, such as polythionates and thiosulfate, are commonly oxidized to sulfite prior to oxidation to sulfate by both abiotic and biotic pathways (Williamson and Rimstidt, 1994). A likely condition for the incorporation of O_2 into intermediate sulfoxyanions during pyrite oxidation is therefore the release of partially oxidized sulfur into an oxygenated solution leading to the final oxidation to sulfate.

However, at low pH < 5, partially oxidized sulfur species remain bonded to the pyrite surface until oxidation is complete and only sulfate is released into solution (e.g., McKibben and Barnes, 1986; Moses et al., 1987; Bonnissel-Gissinger et al., 1998; Rimstidt and Vaughan, 2003). Consequently, the electrochemical model does not accurately describe the role of O_2 or H_2O_2 in the formation of dissolved sulfate during the oxidation of pyrite, since it allows only H_2O-derived oxygen to contribute to product sulfate. It has been hypothesized that a free radical pathway is responsible for the incorporation of O_2 or H_2O_2-derived oxygen into product sulfate. This mechanism involves hydroxyl radicals ($HO^{\bullet}$) produced by the decomposition of H_2O_2 that can be directly attached to the sulfur site on the pyrite surface. The $HO^{\bullet}$ can be produced not only by H_2O_2 dissociation but also by reaction of O_2 with Fe^{2+} in a Fenton-type reaction path, a mechanism proposed by Lowson (1982) and reiterated by Rimstidt and Vaughan (2003). By studying pyrite oxidation by H_2O_2 under anoxic conditions it is possible to test this hypothesis.

3. EXPERIMENTAL

3.1. Materials and methods

This study follows a similar protocol to that described by Lefticariu et al. (2006). Pyrite from quartz–pyrite veins from the Park City district of Utah was first characterized by X-ray diffraction, ICP-MS, and bulk sulfur isotope analyses. Park City pyrite contained about 3 wt% impurities, mainly quartz. Mechanical crushing of pyrite crystals creates chemically active sites on edges, corners, and surface defects (Sasaki, 1994) resulting in artificially accelerated oxidation of pyrite. For this reason, massive composite crystals of Park City pyrite were dismembered and individual intact pyrite crystals were hand picked. Prior to each set of experiments, pyrite crystals were freshly ground without water in an agate mortar by hand, followed by sieving and separation of the 100–150 μm grain size fraction. The 100–150 μm pyrite fraction was then submersed in deoxygenated water in an ultrasonic bath to disaggregate and suspend smaller particles, the supernatant was decanted, and pyrite was briefly acid-washed with deoxygenated 0.1 M HNO_3. After repeated rinsing with deoxygenated deionized (DI) water, the pyrite was dried at room temperature under N_2 prior to loading of aliquots into silica ampoules. All reactions were performed in silica tubes from Quartz Plus Inc. The 15 mm o.d. tube stock was cut into 15 cm lengths. One end was sealed with a torch, and a 9 mm o.d. quartz extension tube was fitted to the other end, resulting in reaction ampoules with a final volume of ~30 mL. Tubes were washed with dilute detergent, rinsed repeatedly with DI water, and baked for 24 h at 500 °C. Each tube was used only once.

Standards and reagents were prepared using deoxygenated DI water from Milli-Q/Milli-Q Ultra Plus (>18 MΩ cm^{-1}) with a UV photo-oxidation water system. DI waters were deoxygenated by purging with ultra-pure argon (Ar) for at least 2 h. Because Milli-Q DI water also contains UV-produced oxidants, following initial Ar purging, water was boiled under Ar atmosphere for 3–4 h and purged a second time with ultra-pure Ar for additional 2 h. Our previous study has shown that this method is efficient in producing oxidant-free solutions (Lefticariu et al., 2006). Control experiments completed in this way at 100 °C containing only pyrite and DI water at neutral pH showed no alteration products even after 6 months of reaction, suggesting low or lack of reactivity of pyrite in the absence of oxidants.

An aliquot of 60 ± 0.1 mg of freshly prepared pyrite was loaded into an ampoule, followed immediately by evacuation to a pressure $<10^{-2}$ Pa in connection with a vacuum

line. After temporarily closing the stopcock connection to the vacuum line, an aliquot of 5 mL of deoxygenated DI water was injected into the evacuated ampoule through a septum port. The water in the ampoule was frozen by submersing the lower end of the ampoule into liquid nitrogen. Evacuation of the ampoule was followed by disconnecting from the vacuum, thawing, re-freezing, and repeated evacuation in order to remove traces of O_2 that may have been initially dissolved in water and ice. Subsequently, an aliquot of 5 mL of H_2O_2 solution (prepared by diluting Fisher Brand 50 wt% hydrogen peroxide with DI water and purged with Ar before use) was injected through the septum into the cold ampoule where the H_2O_2 was promptly frozen on top of the frozen water before any mixing and reaction could occur. The vacuum connection was re-established, residual incondensable gases were evacuated, and the ampoule was sealed at its 9 mm o.d. neck with a torch. Upon initial thawing of the reaction mixture, the H_2O_2 solutions were 0.2 M. Sealed ampoules were quickly brought to a designated experimental temperature in an oven or refrigerator and kept at temperatures from 4 to 150 °C for 7 or 14 days. Each temperature was maintained with an accuracy of ±1 °C. At the end of experiments above 25 °C, ampoules were immersed in ice water to quench the reaction and to stabilize reaction products and remaining reactants.

3.2. Sequential extraction of oxygen species

Each FeS_2–H_2O_2–H_2O experiment yielded data on pH, sulfur speciation, and concentration of sulfur species in the final solution. Experiments at each temperature were performed in parallel sets of ampoules. At the end of each experiment, one tube of each set of duplicates was attached to a tube cracker (DesMarais and Hayes, 1976) and opened in connection to a vacuum line. The only detected product gas was molecular oxygen which was collected in the vacuum line after passage through cryogenic traps and a Toepler pump. The loss of water vapor from the ampoule was minimized by opening the connecting valve to the vacuum line only briefly and intermittently to expand the O_2 repeatedly into the larger volume of the vacuum line from where the Toepler pump collected the O_2 into a manometer for volumetric yield determination, and from there into 9mm o.d. Pyrex® tubes. Each opened ampoule was subsequently removed from the tube cracker, the pH of the solution was measured, and aliquots of the liquid were used to (i) ion-chromatographically analyze the sulfur speciation and (ii) determine the $\delta^{18}O_{H_2O}$ value of the water. Solution pH values were collected and recorded after calibration (4 and 7 pH buffers) with a pH glass electrode (Radiometer XG250) coupled with an Orion® Benchtop 250A pH/mV meter.

Speciation and concentrations of sulfur species were determined on aliquots of supernatant after passage through a 0.22 μm filter (Nalgene 190-2520). Aqueous sulfur speciation was determined ion chromatographically on a Dionex analyzer ICS-2000 using aqueous potassium hydroxide solution as eluent generator and an IonPack AS11-HC column.

Sequential extraction of oxygen species yielded two operationally defined fractions that were extracted from the second set of ampoules: the aqueous sulfate (S_{aq}) fraction and the water-soluble sulfate (S_{ws}) fraction. Pre-baked and dried 0.22 μm pore-size quartz–fiber filters (Whatman, QM-A) were used to separate the filtrate from the solid residue. The S_{aq} fraction in the filtrate was precipitated as barium sulfate ($BaSO_4$) by addition of 1.2 M $BaCl_2$ solution. $BaSO_4$ precipitates were extensively washed with Millipore water, air-dried overnight at 80 °C, and used for determination of $\delta^{18}O_{SO_4}$ values. The filter and residue were returned to the silica ampoule and 20 mL of deoxygenated DI water were added. Ampoules were capped and mixed on a shaking table for 2 h. After shaking, supernatant solution and solid residue were separated by filtration. The second filtrate included water-soluble sulfate from minerals that had been precipitated on the walls of the tube and on pyrite surfaces. This second soluble sulfate fraction was recovered as $BaSO_4$ by addition of 1.2 M $BaCl_2$ solution to the filtrate. Recovered $BaSO_4$ was washed with Millipore water, dried, and retained for isotope analysis.

3.3. Oxygen isotope analyses

The stable isotope ratios of oxygen of the starting and final waters, S_{aq}, S_{ws}, and molecular oxygen are expressed in routine $\delta^{18}O$ notation in ‰ relative to VSMOW (Craig, 1957; Coplen, 1996):

$$\delta^{18}O = (R_{sample} - R_{standard}) \times 1000/R_{standard}(‰) \quad \text{(R6)}$$

R_{sample} and $R_{standard}$ refer to the $^{18}O/^{16}O$ ratios in sample and standard, respectively. A Thermo Finnigan Delta Plus XP mass spectrometer equipped with a Gasbench II, manual dual-inlet system, and Costech elemental analyzer was used to determine oxygen isotopic compositions of solid, aqueous, and gaseous analytes.

3.3.1. Water

The isotopic composition of water ($\delta^{18}O_{H_2O}$) was measured at the beginning and end of each experiment using the technique described by Epstein and Mayeda (1953), by introducing a small volume of carbon dioxide into the headspace of a capped glass vessel that also contained 2 mL of the aqueous solution. The mixture equilibrated for 24 h in a thermostat at 30 °C before CO_2 was admitted from the Gasbench into the ion source. The oxygen isotopic compositions of H_2O present in 0.2 M aqueous peroxide solutions were measured in the same way. $\delta^{18}O_{H_2O}$ values were normalized to the oxygen isotope ratios of two laboratory reference waters, which were directly calibrated with VSMOW and SLAP. The precision (1σ) of the $\delta^{18}O_{H_2O}$ data, on the basis of replicate analyses of the laboratory reference waters, was estimated at ±0.05‰.

3.3.2. Hydrogen peroxide

In order to (i) evaluate the isotopic fractionation associated with oxygen disproportionation during the decomposition of H_2O_2, and (ii) determine the $\delta^{18}O_{H_2O_2}$ value of 100% H_2O_2, we measured the oxygen isotopic composition of both water ($\delta^{18}O_{H_2O}$) and molecular oxygen ($\delta^{18}O_{O_2}$) produced during complete thermal decomposition of 100% H_2O_2 for mineral-blank experiments according to the following reaction:

$$H_2O_2 \rightarrow H_2O + 1/2O_2 \quad (R7)$$

We prepared 100% H_2O_2 by evaporating about 70 vol% of ~50 mL of the initial 50% H_2O_2 aqueous stock solution in the vacuum chamber of a freeze-dryer. The concentration of the residual viscous 100% H_2O_2 was verified by measuring the solution density reaching 1.46 g/mL. An aliquot of freshly prepared 100% H_2O_2 was transferred into a quartz tube under dry N_2 and immediately frozen by immersion into liquid nitrogen. After connecting the tube to a vacuum line and evacuating the headspace, the connecting stopcock to the vacuum line was closed. The H_2O_2 was thawed and gently warmed resulting in quantitative decomposition. O_2 was admitted to the vacuum line, passed through cryogenic traps for purification, and was finally quantified volumetrically after collection with a Toepler pump. H_2O from decomposition of H_2O_2 was first collected in a cryogenic trap at liquid N_2 temperature, and was later thawed and transferred to a closed ampoule for H_2O–CO_2 equilibration in order to determine $\delta^{18}O_{H_2O}$ as described in Section 3.3.1.

O_2 was admitted to the mass-spectrometer dual-inlet system for determination of its $\delta^{18}O_{O_2}$ value. For calibration we used commercial ultra-high purity grade oxygen (99.996%, Indiana Oxygen Co.) with an $\delta^{18}O_{O_2}$ value of −12.1‰, which was calibrated against VSMOW and SLAP standards. The oxygen isotopic composition of water was determined by CO_2 equilibration using the technique described by Epstein and Mayeda (1953). The mixture equilibrated for 24 h at 25 °C before CO_2 was collected and admitted to the mass-spectrometer dual-inlet system. The oxygen isotope composition of CO_2 was based on a reference gas calibrated against VSMOW and SLAP standards. The precision (1σ) of the $\delta^{18}O$ analyses of O_2 was estimated at ±0.03‰.

3.3.3. Sulfate

Sulfate was precipitated from solutions as $BaSO_4$ by addition of $BaCl_2$ to the filtered solutions. Selected $BaSO_4$ precipitates where checked for purity of $BaSO_4$ by XRD. The oxygen isotopic composition $\delta^{18}O_{SO_4}$ of $BaSO_4$ was determined with a Delta Plus XP mass-spectrometer equipped with an on-line elemental analyzer (reductive TC/EA). For stable oxygen isotope ratio measurements, approximately 200 μg of $BaSO_4$ and ~1–2 mg of graphite powder (Fisher Scientific) were loaded into a silver cup and reacted on-line in a TC/EA elemental analyzer at a flash temperature of 1450 °C. Produced CO gas was swept in a He carrier gas stream into the ion source. The oxygen isotopic compositions of international sulfate standards used in this study are IAEA–NBS 127 = +8.6‰, IAEA–SO_5 = +12‰, and IAEA–SO_6 = −11.3‰ versus VSMOW (Böhlke et al., 2003). The overall analytical reproducibility for sulfate oxygen was ±0.3 ‰.

4. RESULTS

4.1. Chemistry, mineralogy, and morphology of pyrite oxidation

No gaseous sulfur species were detected in the headspace of the reaction ampoules from any experiment. Molecular oxygen was the only gaseous product recovered. The yield of O_2 collected at the end of two-week experiments decreased with increasing temperature, with yields similar to values reported by Lefticariu et al. (2006) (Fig. 1a). Initial pH values of H_2O_2/H_2O mixtures after out-gassing were ~5.8 at room temperature. The respective final pH values at the end of the experiments were dependent on the reaction temperatures of the experiments, with values between pH 2.8 for experiments at 4 °C and pH 1.7 for experiments at 150 °C (Fig. 1b). These low pH values are similar to those reported from many acid mine waters (Jambor and Blowes, 1994; Banks et al., 1997; Nordstrom and Alpers, 1999; Jambor et al., 2003).

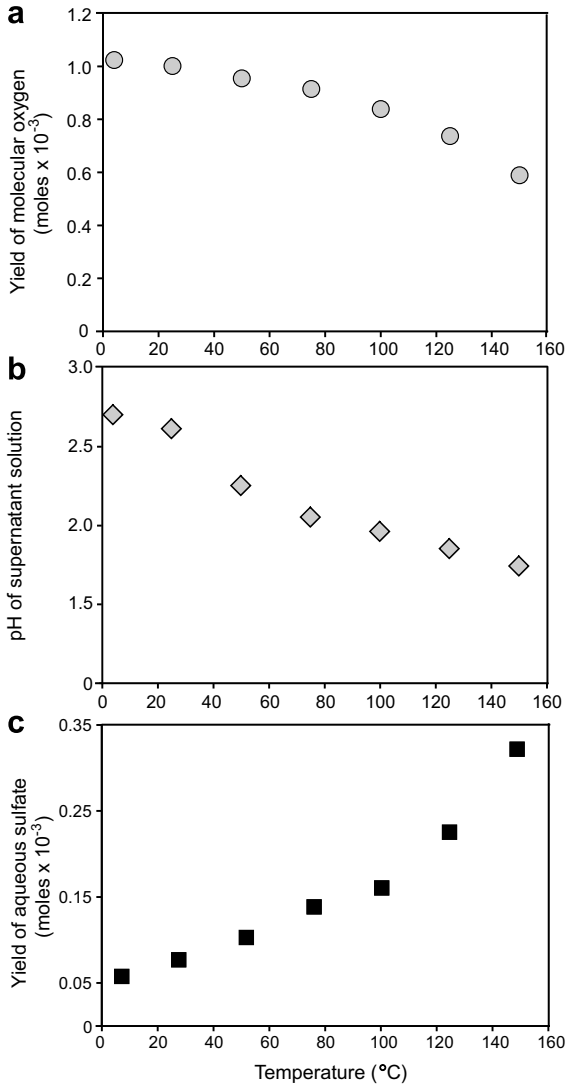

Fig. 1. (a) Yield of molecular oxygen recovered from 0.2 M H_2O_2 pyrite oxidation experiments run for 14 days at temperatures from 4 to 150 °C. (b) Variation of pH values in supernatant solution from 0.2 M H_2O_2 pyrite oxidation experiments run for 14 days at temperatures from 4 to 150 °C. All pH measurements were performed at room temperature. (c) Yield of aqueous sulfate recovered from 0.2 M H_2O_2 pyrite oxidation experiments run for 14 days at temperatures from 4 to 150 °C.

Sulfate was the only sulfur species detected by ion chromatography in the supernatant solutions. Thiosulfate or sulfite concentrations, if present, being below detection limits. Yields of aqueous sulfate increased exponentially with increasing temperature of reaction (Fig. 1c), with overall yields similar to those reported by Lefticariu et al. (2006).

A detailed mineralogical assessment of solid reaction products was reported by Lefticariu et al. (2006). SEM, XRD, and optical microscopic methods identified iron oxyhydroxysulfates, such as rhomboclase, hydroniumjarosite, and kornelite in many experiments. Mineralogical composition and temperature of reaction showed no significant correlation. XRD spectra of the solid products showed peaks attributed to hematite Fe_2O_3, which was detected only in high-temperature experiments (Lefticariu et al., 2006). Finely crystallized hematite with its bright red color was an easily distinguished product in high-temperature experiments. Increased production and larger grain size of hematite were observed with increasing temperature and reaction time. This observation is corroborated by XRD spectra showing characteristic peaks of hematite from experiments at $\geqslant 100$ °C. The crystallization of hematite may be promoted by high temperature and a steady supply of dissolved iron from pyrite oxidation. Absence of iron hydroxide signals in the X-ray diffractograms cannot preclude the existence of Fe oxyhydroxides in the tubes as nanoparticles, colloidal materials or amorphous phases (Banfield and Hengzhong, 2001). However, the low pH < 3 values of supernatant solutions and high SO_4^{2-} concentrations in our experiments favor the formation of Fe oxyhydroxysulfates and may also explain relatively high amounts of Fe oxyhydroxysulfates collected at the end of H_2O_2–pyrite experiments (Lefticariu et al., 2006).

4.2. Oxygen isotope results

Oxygen isotope ratios of the various starting materials and products of pyrite oxidation are listed in Tables 1 and 2, and plotted in Figs. 2 and 3. The following paragraphs highlight individual data sets.

Table 1
Oxygen isotope composition of starting materials for H_2O_2-pyrite experiments

Waters and dilutions	$\delta^{18}O$ (VSMOW, ‰)	$\delta^{18}O$ standard deviation	No. of repeat analyses
Bloomington water	−9.4	0.08	$n = 5$
Canada water	−17.4	0.15	$n = 5$
Miami water	−1.2	0.07	$n = 5$
Water in 50 wt% H_2O_2 stock solution	−7.2	0.07	$n = 5$
Initial 0.2 M H_2O_2 diluted with Bloomington water	−8.9	0.2	$n = 8$
Initial 0.2 M H_2O_2 diluted with Canada water	−15.1	0.25	$n = 6$
Initial 0.2 M H_2O_2 diluted with Miami water	−0.5	0.2	$n = 6$

4.2.1. Oxygen isotopic composition of H_2O

In all H_2O_2–pyrite oxidation experiments, aqueous H_2O_2 solutions were used with an initial concentration of 0.2 M H_2O_2, representing 1.34 wt% H_2O_2 in the initial reaction fluid. The oxygen isotopic composition of water in the aqueous 50% H_2O_2 stock solution (Fisher Scientific) was $\delta^{18}O_{H_2O} = -7.2 \pm 0.07$‰ (Table 1). Two isotopically different waters were deoxygenated following the protocol presented in Section 3.1 and used to prepare diluted 0.2 M H_2O_2 solutions, with resulting $\delta^{18}O_{H_2O}$ values of -8.9 ± 0.15‰ for the 'Bloomington water' in high-^{18}O experiments (Experiment 1) and -15.1 ± 0.2‰ for the 'Canadian water' in low-^{18}O experiments (Experiment 2) (Tables 1 and 2). $\delta^{18}O_{H_2O}$ values of final solutions measured at the end of the experiments ranged between −9.1‰ and −8.7‰ for high-^{18}O experiments, and between −15.3‰ and −14.8‰ for low-^{18}O experiments (Table 2). Final $\delta^{18}O_{H_2O}$ values of supernatant solutions do not show any apparent correlation with reaction temperatures. Instead, they maintained a close isotopic similarity, within experimental error, with their respective initial $\delta^{18}O_{H_2O}$ values for low-^{18}O and high-^{18}O experiments. Obviously, the overwhelming abundance of water and the large oxygen molar ratio H_2O/H_2O_2 of 139/1 in the initial 0.2 M H_2O_2 solution limited the isotopic influence of reacted water or newly generated H_2O from the decomposition of H_2O_2 on bulk $\delta^{18}O_{H_2O}$.

4.2.2. Oxygen isotopic composition of O_2 from decomposition of hydrogen peroxide

Isotopic disproportionation of peroxide oxygen forming two stable products H_2O and O_2 is not the only factor influencing $\delta^{18}O_{H_2O}$ and $\delta^{18}O_{O_2}$ values. Kinetic isotope effects are additionally expected in catalytic reactions during H_2O_2 decomposition in aqueous solutions (e.g., Cahill and Taube, 1952; Dole et al., 1952). Intermediate reactive oxygen-bearing molecules, ions or radicals could isotopically exchange with other oxygen pools present in the aqueous solution. For example, the $\delta^{18}O_{O_2}$ value of generated O_2 could be influenced by the $\delta^{18}O$ values of ambient water. Isotopic exchange could further depend on the presence of catalysts (e.g., platinum). To evaluate this hypothesis, we decomposed H_2O_2 in aqueous solutions with different initial $\delta^{18}O_{H_2O}$ values using different catalysts and isotopically compared the produced O_2. The original 50% H_2O_2 stock solution was diluted for separate experiments with isotopically distinct waters to 0.2 M H_2O_2. The resulting reactant waters had $\delta^{18}O_{H_2O}$ values of −15.1‰ for 'Canadian water' experiments with ^{18}O-depletion and −0.5‰ for 'Miami water' experiments with ^{18}O-enrichment (Table 1). Platinum wire and powdered $KMnO_4$ were used to facilitate the decomposition of H_2O_2. Oxygen gas released during the exothermic decomposition of H_2O_2 was collected following a similar protocol as described in Section 3.3.2. Consistent isotopic results were obtained in all cases with an average $\delta^{18}O_{O_2}$ value of $+47.5 \pm 0.4$‰ ($n = 8$). The small differences were not significantly related to initial $\delta^{18}O_{H_2O}$ values or the use of Pt or $KMnO_4$. These results suggest that O_2 is derived exclusively from H_2O_2 according to reaction (R7), and that the generated O_2 does not

Table 2
Oxygen isotope composition of magnetic or hematite starting materials

Experiment No.[a]	Temp. (°C)	$\delta^{18}O$ (‰)					Calculated % of H_2O-derived oxygen in S_{aq} fraction[b]
		Starting water ($H_2O_{initial}$)	Residual water (H_2O_{final})	Aqueous sulfate (S_{aq}) fraction	Water-soluble sulfate (S_{ws}) fraction	Molecular oxygen (O_2)	
Experiment 1: 7 days							
A # 12B	4	−8.93	−8.83	19.22	18.04	47.90	0.37
	25	−8.93	−8.72	16.37	16.34	47.30	0.43
	50	−8.93	−8.90	7.26	6.68	48.10	0.64
	75	−8.93	−9.12	−2.53	−2.29	48.40	0.86
	100	−8.93	−8.90	−3.78	−3.56	47.30	0.88
	125	−8.93	−9.05	3.97	3.51	48.27	0.71
	150	−8.93	−8.80	6.23	6.68	48.54	0.66
Experiment 1: 14 days							
A # 13B	4	−8.93	−8.89	18.29	18.85	47.81	0.39
	25	−8.93	−8.91	15.95	15.64	48.06	0.44
	50	−8.93	−8.98	7.89	7.43	48.73	0.62
	75	−8.93	−9.15	−1.29	−1.65	47.62	0.83
	100	−8.93	−8.80	−4.06	−4.20	48.50	0.89
	125	−8.93	−9.05	3.28	3.17	48.40	0.73
	150	−8.93	−8.87	5.81	6.15	47.50	0.67
Experiment 2: 7 days							
A # 12C	4	−15.41	NA	15.49	13.22	NA	0.39
	25	−15.41	−14.85	11.37	11.26	48.17	0.47
	50	−15.41	NA	2.53	2.18	NA	0.65
	75	−15.41	NA	−5.77	−5.67	NA	0.81
	100	−15.41	NA	−9.27	−8.82	NA	0.88
	125	−15.41	NA	−3.80	−3.55	NA	0.77
	150	−15.41	NA	−0.34	−1.09	NA	0.70
Experiment 2: 14 days							
A # 13C	4	−15.41	−15.24	14.78	15.41	NA	0.41
	25	−15.41	−15.07	11.63	10.97	47.98	0.47
	50	−15.41	−14.80	1.94	2.29	NA	0.66
	75	−15.41	−15.32	−6.16	−6.24	NA	0.82
	100	−15.41	−14.85	−8.50	−8.72	NA	0.86
	125	−15.41	−15.28	−4.96	−4.55	NA	0.79
	150	−15.41	−15.12	−1.14	−0.19	NA	0.72

NA, not analyzed.

[a] Each experiment was repeated 2 to 6 times.

[b] Estimated percentage of oxygen in sulfate that derives from water, according to $\delta^{18}O_{SO_4} = f_{aq} * \delta^{18}O_{H_2O} + (1 - f_{aq}) * \delta^{18}O_{H_2O}$[2].

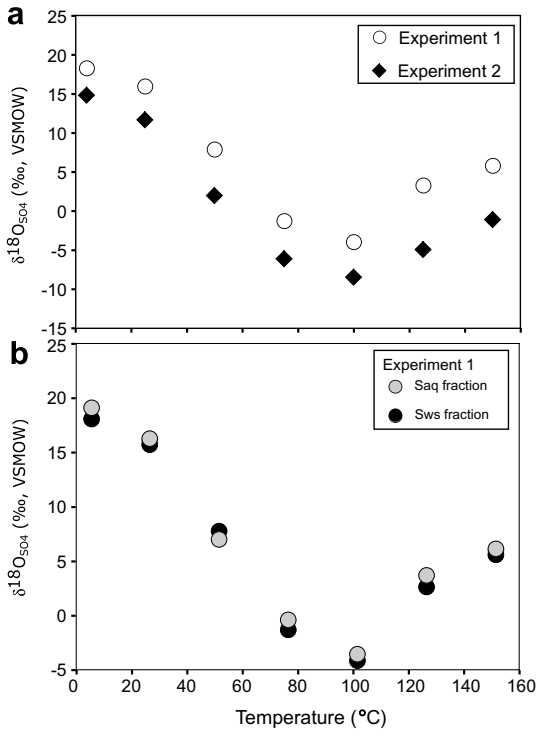

Fig. 2. (a) Oxygen isotope data of aqueous sulfate fractions recovered as $BaSO_4$ from two series of experiments run for 14 days at temperatures from 4 to 150 °C. The $\delta^{18}O_{H_2O}$ values of the 0.2 M H_2O_2 solutions were $-8.9 \pm 0.15‰$ in Experiment 1 and $-15.1 \pm 0.2‰$ in Experiment 2. Similar $\delta^{18}O_{SO_4}$ trends are identified in both series of experiments. (b) Comparison of oxygen isotope data from aqueous (S_{aq}) and water-soluble (S_{ws}) sulfate fractions in Experiment 1. Similar $\delta^{18}O_{SO_4}$ trends of the two sulfate fractions with increasing temperature suggest that the oxygen isotope fractionation between the two sulfate phases is small. Measurement errors are smaller than the plotted symbols.

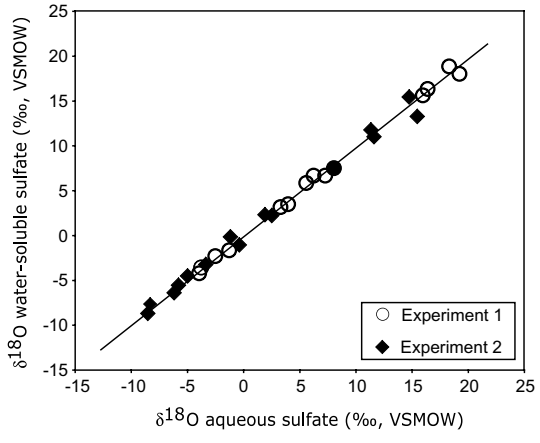

Fig. 3. Comparison of oxygen isotope data from aqueous sulfate (S_{aq} fraction) and water soluble sulfate (S_{ws} fraction). The linear correlation between the two data sets suggests that the oxygen isotope fractionation between the two sulfate phases is small.

exchange isotopically with water oxygen, $KMnO_4$, or any other oxygen-bearing species.

Molecular oxygen was also collected at the end of many pyrite–H_2O_2 experiments (Table 2). Notably, the $\delta^{18}O_{O_2}$ values did not vary with reaction temperature or the duration of experiments (Table 2). The average $\delta^{18}O_{O_2}$ value measured in H_2O_2–pyrite experiments of $+48.1 \pm 0.4‰$ (Table 2) is close to the $\delta^{18}O_{O_2}$ value of $+47.5 \pm 0.4‰$ measured in H_2O_2 decomposition experiments of diluted H_2O_2.

4.2.3. Oxygen isotopic compositions of 100% H_2O_2 and its decomposition products

Six decomposition experiments of 100% H_2O_2 yielded consistent isotopic results for the resulting water ($\delta^{18}O_{H_2O} = +23.4 \pm 0.2‰$) and co-generated molecular oxygen ($\delta^{18}O_{O_2} = +47.6 \pm 0.3‰$). An isotopic mass-balance calculation according to reaction (R7) yields an $\delta^{18}O_{H_2O_2}$ value of $+35.5 \pm 0.3‰$. The oxygen isotope fractionation between O_2 and H_2O measured in these experiments during thermal H_2O_2 decomposition at ~80 °C is $\alpha_{O_2-H_2O} = 1.0236 \pm 0.0002$.

A single batch of a 50% H_2O_2 stock solution was used to prepare our 100% H_2O_2 and all aqueous H_2O_2 dilutions. The striking similarity of $\delta^{18}O_{O_2}$ values from decomposition of 100% H_2O_2 ($\delta^{18}O_{O_2} = +47.6 \pm 0.3‰$, $n = 6$) and from decomposition of dilute aqueous solutions of the 50% H_2O_2stock solution ($\delta^{18}O_{O_2} = +47.5 \pm 0.4‰$, $n = 8$) suggests that no significant $^{18}O/^{16}O$ Rayleigh fractionation of H_2O_2 occurred during preparation of 100% H_2O_2 in a freeze dryer's vacuum chamber via partial evaporation of 50% H_2O_2 stock solution. More importantly, we can adopt our experimentally determined $\delta^{18}O_{H_2O_2}$ value of 100% H_2O_2 for all dilute H_2O_2 solutions that were used in pyrite oxidation experiments.

4.2.4. Oxygen isotopic composition of sulfates

$\delta^{18}O_{SO_4}$ values of aqueous (S_{aq}) and water-soluble (S_{ws}) sulfate fractions are listed in Table 2 and plotted in Figs. 2 and 3. Regardless of experimental conditions, sulfate produced during pyrite oxidation by H_2O_2 was always enriched in ^{18}O relative to water. Measured $\delta^{18}O_{SO_4}$ values of aqueous sulfate range from +19.2‰ to −4.1‰ in Experiment 1 (using relatively ^{18}O-enriched water) and from +15.5‰ to −9.3‰ in Experiment 2 (using relatively ^{18}O-depleted water) (Fig. 2a). This relationship between $\delta^{18}O_{H_2O}$ and $\delta^{18}O_{SO_4}$ demonstrates that some oxygen atoms in newly formed sulfate derive from H_2O under the experimental conditions of pyrite oxidation. The evidence confirms results from our previous study (Lefticariu et al., 2006) where oxygen mass balance calculations indicated that H_2O_2 could not be the sole source of oxygen in sulfate during pyrite oxidation.

$\delta^{18}O_{SO_4}$ values indicate a complex relationship with temperature, with $\delta^{18}O$ values first decreasing systematically in experiments from 4 to 100 °C, followed by a surprising trend reversal above 100 °C (Fig. 2a and b). Values of $\delta^{18}O_{SO_4}$ for the S_{ws} fraction are similar or identical to $\delta^{18}O_{SO_4}$ values of the S_{aq} fraction, and both fractions express the same general trend with increasing temperature (Table 2), suggesting little or no oxygen isotope fractionation between the two sulfate phases (Fig. 3). A direct scanning electron-microscopic morphological comparison

among different sulfate mineral phases on pyrite surfaces was not possible due to the micron to submicron size of mineral aggregates (Lefticariu et al., 2006). No isotopic trend over time has been established by $\delta^{18}O_{SO_4}$ values from one- and two-week experiments utilizing isotopically distinct waters (Fig. 3).

5. DISCUSSION

5.1. Reaction pathways

Mechanisms and rates of pyrite oxidation by O_2 and Fe^{3+} have been the topic of previous studies, particularly in the temperature range that is typical for acid mine drainage (Goldhaber, 1983; McKibben and Barnes, 1986; Williamson and Rimstidt, 1994; Kamei and Ohmoto, 1999; Rimstidt and Vaughan, 2003). Oxidation of pyrite by H_2O_2 increases the level of complexity of the overall system due to the formation of reactive oxygen species during decomposition of H_2O_2, such as hydroxyl radicals $HO^{\cdot}$ (where $^{\cdot}$ denotes an unpaired electron), superoxide ion radicals $O_2^{\cdot -}$, and hydroperoxy radicals $HO_2^{\cdot}$ (McKibben and Barnes, 1986; Lefticariu et al., 2006). Reactions of reactive oxygen species in solution and at the surface of pyrite are highly complex. The following paragraphs discuss pertinent reactions that could occur in the pyrite–H_2O_2 system. Individual reactions are given acronyms according to Table 3.

Hydrogen peroxide in aqueous solution at room temperature suffers spontaneous decomposition at a rate of ~1% per year. The rate of decomposition is dependent on the concentration of H_2O_2, temperature, pH, and the abundance of stabilizers and impurities, e.g., metal ions (Stefanic and LaVerne, 2002).

Thermal decomposition of H_2O_2 involves O–O bond cleavage and results in two $HO^{\cdot}$ radicals according to reaction T1.1 (Table 3), followed by two sequential reactions T1.2 and T1.3 (Hiroki and LaVerne, 2005). The overall stoichiometry is according to reaction (R7) in which one O_2 molecule is produced for every two decomposed H_2O_2 molecules. Various solid surfaces are known to promote the formation of free radicals as intermediates during the catalytic decomposition of H_2O_2 (Weiss, 1935; Weiss and Humphrey, 1949; Abbot and Brown, 1990; Lin and Gurol, 1998; Petrik et al., 2001; Balbuena et al., 2006). On metal surfaces, the dissociation of H_2O_2 is initiated when an electron is donated from the uncharged metal substrate (M) to the H_2O_2 molecule, followed by O–O bond cleavage and the formation of a hydroxyl radical $HO^{\cdot}$ and a hydroxyl ion

Table 3
Primary reactions in FeS_2–H_2O–H_2O_2 system and rate constants for individual reactions

Reaction no.	Reaction	Rate constant mol^{-1} s^{-1}	Literature source
I. H_2O_2 thermal decomposition			
T1.1	$H_2O_2 \rightarrow 2\ HO^{\cdot}$	1.2×10^7	Elliot et al. (1990)
T1.2	$HO^{\cdot} + H_2O_2 \rightarrow HO_2^{\cdot} + H_2O$	3.3×10^7	Buxton et al. (1988)
T1.3	$2HO_2^{\cdot} \rightarrow H_2O + O_2$	1.7×10^7	Elliot et al. (1990)
II. H_2O_2 decomposition on metal surfaces			
T2.1	$M + H_2O_2 \rightarrow M^+ + OH^- + HO^{\cdot}$		Weiss (1952)
T2.2	$HO^{\cdot} + H_2O_2 \rightarrow H_2O + O_2^{\cdot -} + H^+$		Haber and Weiss (1934)
T2.3	$H_2O_2 + O_2^{\cdot -} \rightarrow HO^{\cdot} + H_2O + O_2$		Haber and Weiss (1934)
T2.4	$M^+ + O_2^{\cdot -} \rightarrow M + O_2$		Weiss (1952)
T2.5	$M + HO_2^{\cdot} \rightarrow M^+ + HO_2^-$		Weiss (1952)
III. Reactive oxygen radical reactions			
T3.1	$H_2O_2 + HO^{\cdot} \rightarrow HO_2^{\cdot} + H_2O$	3.1×10^7	Buxton et al. (1988)
T3.2	$HO_2^{\cdot} + HO_2^{\cdot} \rightarrow H_2O_2 + O_2$	8.3×10^5	Rush and Bielski (1985)
T3.3	$HO_2^{\cdot} + O_2^{\cdot -} + H^+ \rightarrow H_2O_2 + O_2$	9.7×10^7	Rush and Bielski (1985)
T3.4	$HO_2^{\cdot} + HO^{\cdot} \rightarrow H_2O + O_2$	8.9×10^9	Moffett and Zika (1987)
T3.5	$HO^{\cdot} + HO^{\cdot} \rightarrow H_2O_2$	5.2×10^9	Rush and Bielski (1985)
IV. Fe^{II} oxidations			
T4.1	$Fe^{2+} + H_2O_2 \rightarrow Fe^{3+} + HO^{\cdot} + OH^-$	5.7×10^2	Rush and Bielski (1985)
T4.2	$Fe^{2+} + HO^{\cdot} \rightarrow Fe^{3+} + OH^-$	3.2×10^8	Stuglik and Zagorski (1981)
T4.3	$Fe^{2+} + HO_2^{\cdot} \rightarrow Fe^{3+} + HO_2^-$	6.6×10^6	Haber and Weiss (1934)
T4.4	$Fe^{2+} + HO^{\cdot} + H^+ \rightarrow Fe^{3+} + H_2O$	5.6×10^6	Haber and Weiss (1934)
T4.5	$Fe^{2+} + HO_2^{\cdot} + H^+ \rightarrow Fe^{3+} + H_2O_2$	6.6×10^6	Haber and Weiss (1934)
T4.6	$Fe^{2+} + O_2 \rightarrow O_2^{\cdot -} + Fe^{3+}$	1.2×10^4	King (1998)
T4.7	$Fe^{2+} + O_2^{\cdot -} + 2H^+ \rightarrow Fe^{3+} + H_2O_2$	1×10^7	Rush and Bielski (1985)
V. Fe^{IV}-oxo complex mechanism			
T5.1	$Fe^{2+} + H_2O_2 \rightarrow FeO^{2+} + H_2O$		Dunford (2002)
T5.2	$FeO^{2+} + H_2O_2 \rightarrow Fe^{2+} + O_2 + H_2O$		Dunford (2002)
T5.3	$FeO^{2+} + Fe^{2+} + 2H^+ \rightarrow 2Fe^{3+} + H_2O$		Dunford (2002)
VI. Fe^{III} reductions			
T6.1	$Fe^{3+} + H_2O_2 \rightarrow Fe^{2+} + HO_2^{\cdot} + H^+$	2.6×10^{-3}	Kwan and Voelker (2002)
T6.2	$Fe^{3+} + HO_2^{\cdot} \rightarrow Fe^{2+} + O_2 + H^+$	3.3×10^7	Haber and Weiss (1934)
T6.3	$Fe^{3+} + O_2^{\cdot -} \rightarrow Fe^{2+} + O_2$	1.5×10^8	Rush and Bielski (1985)

OH^- (reaction T2.1 in Table 3). In solution, $HO^\cdot$ initiates a free radical chain reaction, known as the Haber–Weiss cycle (Weinstein and Bielski, 1979), which produces oxygen radicals and molecular oxygen (reactions T2.2 and T2.3). The charged metal surface M^+ can further accept electrons from oxygen radicals to yield molecular oxygen O_2 (reaction T2.4) or hydroperoxy ions HO_2^- (reaction T2.5). These redox reactions on pyrite could affect its surface reactivity and lead to more aggressive oxidation on the surface. SEM photographs of the pyrite surface taken before and after exposure to H_2O_2 support this hypothesis (Fig. 4). Reactive oxygen species generated during H_2O_2 decomposition in solution would subsequently react with H_2O_2 (reaction T3.1) or with each other to form H_2O, H_2O_2, and O_2 (reactions T3.1–T3.5). Similarly, intermediate products from H_2O_2 decomposition would rapidly diffuse from the surface into solution and engage in aqueous reactions.

The decomposition of aqueous H_2O_2 is catalyzed by many compounds, e.g., iron and transition metals. The mechanisms of H_2O_2 decomposition by Fe^{2+}/Fe^{3+} aqueous complexes are still not resolved (Barb et al., 1949; Koppenol and Liebman, 1984; King et al., 1995; Lin and Gurol, 1998; Dunford, 2002; González-Davila et al., 2005). Two reaction pathways have been proposed, namely (i) a free radical pathway with $HO^\cdot$ production, and (ii) a non-free radical pathway involving ferryl ion FeO^{2+} ions. Oxidation of Fe^{2+} by H_2O_2 can occur via a redox mechanism know as Fenton reaction (reaction T4.1), leading to the production of Fe^{3+} ions, hydroxyl ions HO^-, and highly reactive $HO^\cdot$ radicals. In solution, Fe^{2+} can potentially be oxidized by $HO^\cdot$ (reaction T4.2), $HO_2^\cdot$ (reaction T4.3), and dissolved O_2 (reaction T4.4). Competing reactions for Fe^{2+} oxidation can involve H_2O_2 and O_2. The rate constant for oxidation of Fe^{2+} by H_2O_2 at low pH (reaction T4.1) is two orders of magnitude larger than the rate constant for oxidation of Fe^{2+} by O_2 (reaction T4.5). Thus we expect that in a mixed H_2O_2–O_2 solution under similar conditions to our experiments, the oxidation of Fe^{2+} will be mediated mostly by H_2O_2 and to a lesser degree by O_2.

The ferryl ion species FeO^{2+} has been proposed to act as the active species in a non-free radical mechanism of iron-catalyzed decomposition of H_2O_2 (Bray and Gorin, 1932; Kremer, 1999). The initial step in reaction T5.1 produces FeO^{2+} as the active intermediate iron species. Reaction T5.2 takes place when H_2O_2 is available in excess relative to Fe^{2+}, leading to the formation of O_2 and the regeneration of the Fe^{2+} catalyst. However, when Fe^{2+} is in excess, reaction T5.1 is followed by reaction T5.3 terminating chain reactions. According to Dunford (2002) there is no obvious way to kinetically distinguish the free radical mechanism from the iron complex mechanism. Due to the low pH in the present experiments, Fe^{2+} oxidation by $HO^\cdot$ radicals is likely the predominant reaction pathway both on the pyrite surface and in solution (Lefticariu et al., 2006). Future experimental and field studies will be needed to determine if ferryl ions are a significant reactive intermediate or constituent of mineral products in geochemical reactions in Earth's lithosphere.

In addition, back reactions should be considered in which aqueous Fe^{3+} is reduced to Fe^{2+} by various reactive oxygen species. Fe^{3+} can catalyze H_2O_2 decomposition according to reaction T6.1, or it can react with hydroperoxy radicals $HO_2^\cdot$ (reaction T6.2) or with superoxide ion radicals $O_2^{\cdot-}$ (reaction T6.3). In all cases Fe^{2+} is regenerated in solution.

Our experiments represent closed systems where H_2O_2 is neither added nor regenerated and consequently the H_2O_2 concentrations decrease over time due to thermal and catalytic decomposition. Previous studies demonstrated a linear correlation between the rate of H_2O_2 decomposition and reaction temperature from 0 to 150 °C, regardless of pathway and catalyst (Gray, 1959; Croiset et al., 1997; Hiroki and LaVerne, 2002), indicating that the decomposition of H_2O_2 in the presence of different catalysts follows first-order kinetics (Fig. 5). To date, no data have been published on rates of H_2O_2 decomposition on pyrite surfaces. Results from H_2O_2 decomposition experiments in clean Pyrex® glass tubes without any other reactant or catalyst (line 'a' in Fig. 5) provide a lower estimate that would likely need to be revised upward in the presence of pyrite. Extrapolation of these data to the conditions of our pyrite–H_2O_2 experimental systems yields estimates for the half-life of H_2O_2 during thermal decomposition at 4 °C over 30 days, at 25 °C over 20 days, at 50 °C over 7 days, at 75 °C over 18 h, at 100 °C over 30 min, and at 150 °C over 15 min. Hence the H_2O_2-related impact on pyrite oxidation is a function of temperature, with a maximum effect in low-temperature experiments when relatively slowly generated

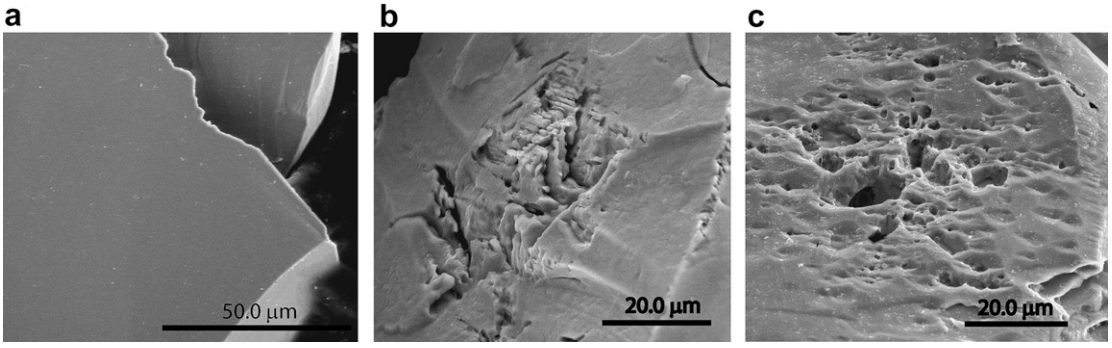

Fig. 4. SEM photomicrographs of (a) acid-cleaned pyrite before exposure to H_2O_2; (b and c) residual pyrite surface at the end of 0.2 M H_2O_2 pyrite oxidation experiments run for 14 days at 50 °C. Dissolution pits on pyrite surfaces are the result of aggressive oxidation reactions by reactive oxygen species resulting from decomposition of H_2O_2.

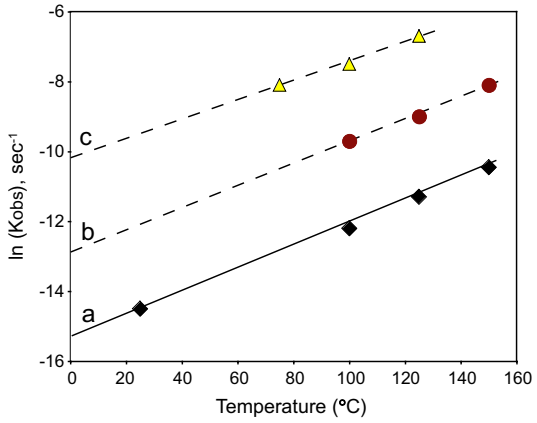

Fig. 5. Arrhenius plot of ln(K_{obs}), the natural logarithm of the thermal decomposition rate coefficient of H_2O_2. ln(K_{obs}) is plotted as a function of temperature for H_2O_2 decomposition (a) in Pyrex® glass tubes with no added catalysts, (b) in the presence of SiO_2 catalyst, (c) in the presence of Al_2O_3 catalyst. Thermal decomposition of H_2O_2 has first-order decay kinetics for the observed loss of H_2O_2. For first-order decay, as described by reaction (R7), the observed loss of H_2O_2 can be written as: $\ln([H_2O_2]/[H_2O_2]_0 = -K_{obs}*t)$. t = residence time, $[H_2O_2]_0$ and $[H_2O_2]$ are the H_2O_2 concentrations before and after heating, respectively. Data from Hiroki and LaVerne (2005).

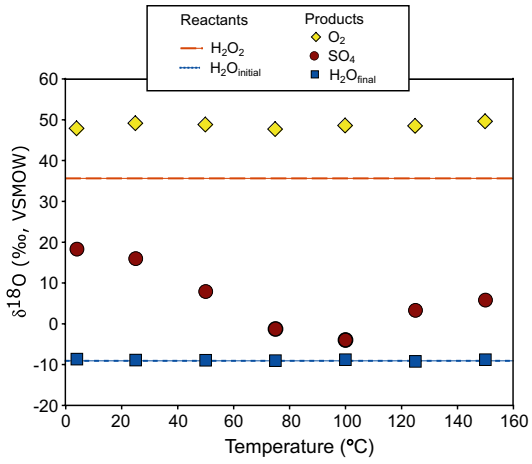

Fig. 6. Summary of oxygen isotope data from 0.2 M H_2O_2 pyrite oxidation experiments run for 14 days at temperatures from 4 to 150 °C.

oxygen radical species have ample time to react with the pyrite surface. In contrast, at high temperatures the time window for attack by H_2O_2-generated oxygen radical species is too short, impairing a relatively larger role to non-radical mechanisms of pyrite oxidation.

In the H_2O–FeS_2–H_2O_2 system, chain reactions between FeS_2, H_2O_2, and their decomposition products provide a supply of oxygen free radicals, O_2 and Fe^{3+} (Table 3). All of these products are expected to act as oxidants for pyrite. The oxidation rates depend upon the relative rates of different processes at different temperatures. The chemical mechanisms of pyrite oxidation by each of these oxidants are different, resulting in potentially different $\delta^{18}O_{SO_4}$ values.

5.2. Interpretation of oxygen isotope values

Oxidation of pyrite by H_2O_2 can be described by the following generalized reaction:

$$FeS_2 + H_2O_2 + H_2O_{initial} \rightarrow Fe^{2+} + SO_4^{2-} + O_2 + H_2O_{final} + \text{residual } FeS_2 \quad (R8)$$

Sulfate is the terminal oxidation product of sulfur from pyrite. Its four oxygen atoms may derive from various sources. The most likely sources and the overwhelmingly largest pools of available oxygen at the initial stage in our experiments are in H_2O and H_2O_2. Other forms of oxygen are present in phosphate that is used as a stabilizer in the 50% H_2O_2 stock solution, and in the silica glass of the tubes, but these substrates are not strongly oxidizing and their extraordinary chemical stability makes their oxygen unavailable for transfer into sulfate. Therefore, differences in $\delta^{18}O$ of the potential oxygen sources H_2O_2 and/or H_2O are exploited in this study to determine the origin of sulfate oxygen (Fig. 6).

Sulfate from our various experiments of pyrite oxidation spans a wide range of $\delta^{18}O_{SO_4}$ values from −3.9‰ to +19.2‰ in Experiment 1 and from −9.3‰ to +15.5‰ in Experiment 2 (Table 2 and Fig. 2a) indicating that sulfate incorporated oxygen in different proportions from both H_2O_2 ($\delta^{18}O_{H_2O_2} = +35.5‰$) and H_2O ($\delta^{18}O_{H_2O} = -8.9‰$) in high-$^{18}O$ experiments, and $\delta^{18}O_{H_2O} = -15.1‰$ in low-^{18}O experiments. At each experimental temperature considered, the limited differences in $\delta^{18}O_{SO_4}$ values between one-week and two-week long isothermal experiments suggest that the mechanisms of pyrite oxidation did not change over the duration of these experiments (Fig. 3). The incorporation of oxygen atoms into sulfate from both H_2O and H_2O_2 calls for more than one mechanism of sulfate formation because no single reaction mechanism in Table 3 can account for dual sourcing of sulfate oxygen from H_2O and H_2O_2.

One of our main objectives is to establish an oxygen isotope mass balance in the FeS_2–H_2O–H_2O_2 system by considering the distribution of oxygen species during pyrite oxidation by H_2O_2 (Fig. 6). Oxygen-containing reactants are the initial water ($H_2O_{initial}$) and hydrogen peroxide (H_2O_2). Oxygen-containing products are the sulfate fractions S_{aq} and S_{ws}, residual water (H_2O_{final}) and molecular oxygen (O_2). We can express $\delta^{18}O_{SO_4}$ in terms of the isotopic mol fraction of oxygen contributed from initial oxygen-donor species H_2O and H_2O_2:

$$\delta^{18}O_{SO_4} = f_{aq} * (\delta^{18}O_{H_2O} + \Delta_{SO_4-H_2O}) + f_{H_2O_2} * (\delta^{18}O_{H_2O_2} + \Delta_{SO_4-H_2O_2}) \quad (R9)$$

where fractions incorporated into sulfate are expressed as f_{aq} for oxygen from H_2O, and $f_{H_2O_2}$ for oxygen from H_2O_2. Isotopic fractionations between sulfate and water $\Delta_{SO_4-H_2O}$ and between sulfate and hydrogen peroxide $\Delta_{SO_4-H_2O2}$ are expressed in ‰.

Simple isotopic mass-balance calculations do not take into account additional complications that may affect $\delta^{18}O_{SO_4}$ values. Different oxygen isotope effects associated with parallel pathways toward sulfate formation may complicate the picture. The limited $\delta^{18}O$ isotopic differences between the various oxygen pools used in our experiments and the number of experiments preclude detailed isotopic distinction among complex parallel pathways.

5.2.1. Oxygen isotope exchange reactions

Experimental studies have shown that non-biological isotope exchange between water and sulfate is negligible under the pH, temperature, and time conditions of our experiments (e.g., Mizutani and Rafter, 1969a,b; Lloyd, 1967, 1968; Chiba and Sakai, 1985). However, no previous study has considered the possibility of oxygen isotope exchange between aqueous sulfate and H_2O_2 or other reactive oxygen species produced during H_2O_2 thermal or catalytic decomposition.

In two sets of mineral-blank experiments we investigated oxygen isotope exchange, whereby 5×10^{-3} mol of sodium sulfate Na_2SO_4 or sodium sulfite Na_2SO_3 were dissolved in 10 mL of 0.2 M H_2O_2 solutions and kept for 2 weeks at temperatures from 4 to 150 °C in oxidizing conditions following identical protocols as in pyrite–H_2O_2 experiments. The H_2O_2 solutions started with initial values of $\delta^{18}O_{H_2O} = -8.9‰$ and $\delta^{18}O_{H_2O_2} = +35.5‰$. Initial oxygen isotope ratios of solid, anhydrous Na_2SO_4 and Na_2SO_3 were $\delta^{18}O_{SO_4} = +12.8‰$ and $\delta^{18}O_{SO_3} = -1.4‰$. At the end of Na_2SO_4–H_2O_2 experiments, the final $\delta^{18}O_{SO_4}$ value of $+12.4 \pm 0.4‰$ was similar to the initial $\delta^{18}O_{SO_4}$ value of $+12.8 \pm 0.4‰$ suggesting that no oxygen isotope exchange took place between sulfate and other oxygen-bearing species (Table 4).

Ion chromatographic measurements at the end of the Na_2SO_3–H_2O_2 experiments showed that sulfite had been completely oxidized to sulfate. The final $\delta^{18}O_{SO_4}$ values did not depend on reaction temperature and displayed similar values averaging $\delta^{18}O_{SO_4} + 11.1 \pm 0.4‰$ (Table 4). Oxidation of sulfite in the Na_2SO_3–H_2O_2 system probably occurred according to the following reaction:

$$SO_3^{2-} + H_2O_2 \rightarrow SO_4^{2-} + H_2O \quad \text{(R10)}$$

Additional experiments at room temperature indicated that reaction (R10) was completed within seconds and the newly formed sulfate did not exchange oxygen with water or H_2O_2. These observations support our hypothesis that sulfate ones formed did not exchange oxygen with H_2O_2 or any other oxygen radical species present in the system. Thus, one or more processes other than oxygen isotope exchange are responsible for the observed trend in $\delta^{18}O_{SO_4}$ values with temperature (Fig. 6), but they provide no information about the chemical identity of relevant reactive species.

5.2.2. Oxygen isotope fractionation between sulfate and water

Abiotic oxidation of pyrite dominated by reaction (R1) showed minimal oxygen isotope fractionation between dissolved sulfate and associated water (Toran and Harris, 1989; Taylor and Wheeler, 1994). In addition, experimental abiotic studies found no oxygen isotope fractionation between (i) sulfate and water associated with the oxidation of Na_2S (Lloyd, 1967), and (ii) between sulfate and water associated with the oxidation of native sulfur (Mizutani and Rafter, 1969b). At pH >3, dissolved intermediate sulfur species remain bonded to pyrite surfaces until oxidation is complete and only sulfate is released into solution (Moses et al., 1987; Bonnissel-Gissinger et al., 1998; Rimstidt and Vaughan, 2003; Todd et al., 2003). It is therefore expected that oxygen isotope fractionation between dissolved sulfate and water during abiotic oxidation of pyrite associated with reaction (R1) is negligible (i.e., $\Delta_{SO_4-H_2O} \approx 0$). This expectation also applies to our sterile experiments, in which solutions with low pH would have prevented the release of intermediate sulfur species (e.g., polythionates, thiosulfates, and sulfite) from the pyrite surface into solution.

Table 4
Oxygen isotopic compositions of starting materials and sulfate products in Na_2SO_4–H_2O_2 and Na_2SO_3–H_2O_2 experiments

Experiment[a] (a)	Temperature (°C)	$\delta^{18}O$ (VSMOW, ‰)	$\delta^{18}O$ standard deviation
Initial Na_2SO_4		12.82	0.18
Residual SO_4^{2-}	4	12.31	0.31
Residual SO_4^{2-}	25	12.46	0.45
Residual SO_4^{2-}	50	11.53	0.28
Residual SO_4^{2-}	75	12.51	0.21
Residual SO_4^{2-}	100	12.72	0.11
Residual SO_4^{2-}	125	12.68	0.17
Residual SO_4^{2-}	150	12.69	0.16
Average $\delta^{18}O_{SO4}$		12.41	0.24
Initial Na_2SO_3		−1.41	0.28
Residual SO_4^{2-}	4	11.65	0.28
Residual SO_4^{2-}	25	10.98	0.09
Residual SO_4^{2-}	50	10.91	0.21
Residual SO_4^{2-}	75	11.05	0.15
Residual SO_4^{2-}	100	10.56	0.11
Residual SO_4^{2-}	125	10.83	0.24
Residual SO_4^{2-}	150	11.53	0.18
Average $\delta^{18}O_{SO4}$		11.07	0.18

[a] Each experiment was repeated 2 to 6 times.

5.2.3. Origin of sulfate oxygen

The oxygen isotope composition of sulfate resulting from pyrite oxidation by H_2O_2 can be expressed as the sum of two fractions, namely the H_2O-derived oxygen fraction (f_{aq}) and the H_2O_2-derived oxygen ($1 - f_{aq}$). In order to calculate f_{aq}, we assume that no isotope fractionation occurs during the transfer of oxygen from water or peroxide into sulfate and use the following equation:

$$\delta^{18}O_{SO_4} = f_{aq} * \delta^{18}O_{H_2O} + (1 - f_{aq}) * (\delta^{18}O_{H_2O_2}) \quad \text{(R11)}$$

In the subsequent calculations, we employ the calculated $\delta^{18}O_{H_2O_2}$ value for hydrogen peroxide (see Section 4.2.3) and the $\delta^{18}O_{H_2O}$ values of the initial aqueous solutions (Table 1). We used the $\delta^{18}O_{SO_4}$ value of the aqueous sulfate

fractions from 14-day experiments (Table 2) because similar $\delta^{18}O_{SO_4}$ values were measured for aqueous and water-soluble sulfate fractions in these experiments (Section 4.2.4.).

$\delta^{18}O_{SO_4}$ values of +15.9‰ in Experiment 1 and +11.6‰ in Experiment 2 let us estimate that ~50% of the oxygen in sulfate derives from H_2O at a reaction temperature of 25 °C (Fig. 7). In the FeS_2–H_2O_2–H_2O system, catalytic decomposition of H_2O_2 produces $HO^{\cdot}$ and other reactive oxygen radicals (Table 3). $HO^{\cdot}$ is known to react rapidly and unselectively with many chemical species (Dorfman and Adams, 1973; Rush and Bielski, 1985; Spinks and Woods, 1990; Druschel et al., 2004; Garrett et al., 2004; Kminek and Bada, 2006), extending to Fe and S sites on pyrite surfaces (Borda et al., 2003). Aqueous Fe^{3+} ions are generated in solution during reactions of Fe^{2+} with reactive oxygen species (e.g., reactions T4.1–T4.7). The reducing back reaction of aqueous Fe^{3+} to Fe^{2+} (reaction T6.1) is an order of magnitude slower than oxidation reactions (Table 3), making Fe^{2+} regeneration a less important process. Chain reactions on pyrite surfaces and in solution generate many different reactive oxygen species that are known to be effective oxidants for pyrite, most importantly $HO^{\cdot}$ and Fe^{3+} (Table 3). These chain reactions are self-sustaining as long as H_2O_2 is present in the system. During pyrite oxidation by H_2O_2, the resulting SO_4^{2-} incorporates H_2O-derived oxygen (through Fe^{3+} oxidation; reaction (R1)) and H_2O_2-derived oxygen (through oxidation by $HO^{\cdot}$ radicals; reaction (R4)). These results indicate that water plays an important role in pyrite oxidation even in the presence of powerful oxidants like H_2O_2 (Fig. 7). At 25 °C the two reaction pathways (R3) and (R4) seem to have equal importance in sulfate production. The following general reaction summarizes the oxidation of pyrite by H_2O_2 at 25 °C:

$$FeS_2 + 10Fe^{3+} + 4H_2O + 2H_2O_2 \rightarrow 11Fe^{2+} + 2SO_4^{2-} + 12H^+ \quad (R12)$$

The fraction of sulfate oxygen that is derived from H_2O increases with rising reaction temperature from ~40% at 4 °C to ~90% at 100 °C (Fig. 7). This trend with increasing temperature runs parallel to increasing rates of H_2O_2 decomposition (Fig. 5), shorter residence time of radicals, and diminishing time of H_2O_2 availability. Thus, from 4 to 100 °C, oxygen incorporation into sulfate is dominated by reaction (R1) with a minor contribution from (R4) until H_2O_2 is consumed. Subsequently, in the absence of H_2O_2 only (R1) remains operative.

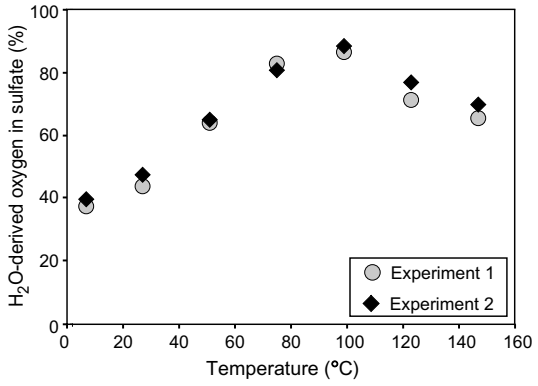

Fig. 7. Comparison of estimated percentage of H_2O-derived oxygen incorporated into sulfate as a function of temperature of reaction. In order to calculate the H_2O-derived oxygen fraction we assume that no isotope fractionation occurs during the transfer of oxygen from water. Data tabulated in Table 2.

The reversal of the $\delta^{18}O_{SO_4}$ trend above 100 °C is puzzling (Fig. 6). Thermal decomposition of H_2O_2 would be completed after ~150 min at 100 °C and after ~75 min at 150 °C, even in the absence of a catalyst (Hiroki and LaVerne, 2005). Extrapolation of the <100 °C low-temperature trend (Fig. 6) gave reason to our expectation that more rapid H_2O_2 decomposition at higher temperatures would further reduce the transfer of H_2O_2-derived oxygen atoms into sulfate. The deviating results above 100 °C (Fig. 7) strongly suggest that one or more different oxygen sources significantly contribute to newly forming sulfate, and/or that different mechanism(s) are operating at higher temperatures.

H_2O and O_2 are the two stable products of H_2O_2 decomposition. The oxygen molar ratio for H_2O/H_2O_2 is 139/1 in the initial 0.2 M H_2O_2 solution and limits the isotopic influence of new H_2O derived from the decomposition of H_2O_2 on bulk $\delta^{18}O_{H_2O}$. On pyrite surface, oxygen sourced from H_2O_2-derived water can be actively involved in reactions and can transfer its oxygen signature to the sulfate. In addition, oxygen sourced from H_2O_2-derived water can be actively involved in reactions in solution as well as on pyrite surfaces for as long as H_2O_2 is present in the system. However, the H_2O_2-derived, new water represents a minor pool of oxygen compared to the pre-existing water in our systems and therefore has a minor role in the overall oxygen isotope budget. Values of $\delta^{18}O_{SO_4}$ are remarkably similar for experiments lasting one or two weeks (Fig. 3), further supporting this hypothesis. In contrast, H_2O_2-derived O_2 with strong ^{18}O-enrichment ($\delta^{18}O_{O_2} = +48.1‰$) could play an important role in sulfate formation at high temperatures. Measured amounts of O_2 at the end of 14-day experiments decreased with increasing reaction temperature, suggesting that O_2 is consumed and incorporated in reaction product(s) (Fig. 1a).

We postulate that the reversed trend for $\delta^{18}O_{SO_4}$ above 100 °C (Fig. 6) is caused by an alternative iron-dependent mechanism allowing the incorporation of O_2 into sulfate during hematite formation. The proposed mechanism involves reactions of Fe^{2+}/Fe^{3+} with O_2 and the oxidative properties of resulting Fe/O_2 complexes. Iron-mediated reactions can be initiated in solution or on pyrite surface by a ferrous iron-oxygen complex such as perferryl ion FeO_2^+ (Bray and Gorin, 1932; Lowson, 1982). Perferryl iron is an intermediate product that can be generated in Fe^{2+}/O_2 or $Fe^{3+}/O_2^{\cdot -}$ reactions (Dunford, 2002):

$$Fe^{2+} + O_2 \leftrightarrow [Fe^{2+}\text{–}O_2 \leftrightarrow Fe^{3+}\text{–}O_2^{\cdot -}] \leftrightarrow Fe^{3+} + O_2^{\cdot -} \quad (R13)$$

FeO_2^+ could nucleate the precipitation of hematite in high temperature experiments after the solution becomes supersaturated with respect to hematite, according to:

$$2Fe^{2+}O = O + H^+ + 6Fe^{2+} \rightarrow Fe_2O_3 + 6Fe^{3+} + OH^- \quad (R14)$$

During hematite Fe_2O_3 formation, FeO_2^+ may interact with the pyrite surface, break the O═O bond, acquire H^+ and attach one OH^- to sulfur sites. Such processes are reasonable considering prior studies which showed that iron oxides are effective catalysts for the oxidation of reactants such as SO_2 in the presence of molecular oxygen (Dunn et al., 1999). According to reaction (R14), the heritage of oxygen atoms in hematite from perferryl-bonded O_2 mandates an isotopic relationship between $\delta^{18}O_{perferryl}$ and $\delta^{18}O_{hematite}$ that may include oxygen fractionation during disproportionation of perferryl to hematite and OH^-, as well as Rayleigh-type fractionation along an incomplete reaction (R14). Recent ^{18}O-labeling studies support this hypothesis by demonstrating that the oxygen in iron oxyhydroxide is derived in large part from O_2 during pyrite oxidation (Usher et al., 2005).

A general reaction describing the oxidation of pyrite at 150 °C and the distribution of oxygen among reactants and products is:

$$FeS_2 + 12Fe^{3+} + O_2 + 9H_2O \rightarrow Fe_2O_3 + 11Fe^{2+} + 2SO_4^{2-} + 18H^+ \quad (R15)$$

We hypothesize that during pyrite oxidation at $\geqslant$100 °C, the resulting SO_4^{2-} incorporates H_2O-derived oxygen through oxidation by Fe^{3+} (reaction (R1)) and H_2O_2-derived oxygen through (i) oxidation by O_2 (reaction (R2)), and (ii) to a lesser extend via oxidation by $HO^\bullet$ (reaction (R4)). Oxygen incorporation into sulfate is therefore dominated by reaction (R1) coupled with a lesser contribution from reaction (R2). The increase in $\delta^{18}O_{SO_4}$ values above 100 °C implies that the fraction of O_2-derived oxygen incorporated in sulfate increases with increasing temperature.

6. CONCLUSIONS

Our results from ^{18}O-labeled experiments clarify mechanisms of pyrite oxidation by H_2O_2 at various temperatures and resolve the sources of oxygen atoms that are incorporated into produced sulfate. Catalytic and thermal decomposition of H_2O_2 in aqueous solution and on pyrite surface results in the formation of reactive oxygen species (e.g., $HO^\bullet$ radicals and O_2) and ion species from pyrite oxidation (e.g., Fe^{3+}). The relative efficiencies of competing oxidation reactions of pyrite by $HO^\bullet$ radicals, O_2, and Fe^{3+} are dependent on temperature. Contrasting $\delta^{18}O$ values of H_2O and H_2O_2 as the two primary sources of oxygen in our experiments allow for discrimination among different mechanisms for the incorporation of oxygen into sulfate. The $\delta^{18}O$ values of sulfate suggest the presence of competing mechanisms for the incorporation of oxygen into sulfate. Low-temperature experiments indicate that H_2O-derived oxygen is incorporated into sulfate via Fe^{3+} oxidation, whereas H_2O_2-derived oxygen is incorporated into sulfate via oxidizing hydroxyl radicals ($HO^\bullet$). With increasing reaction temperatures, the accelerated thermal decomposition and the diminished residence time of H_2O_2 limit the oxygen transfer from H_2O_2 into sulfate. However, at high temperatures the molecular oxygen (O_2) from the decomposition of H_2O_2 seems to become available for pyrite oxidation via perferryl ions FeO_2^+. The proposed mechanism implies that during hematite Fe_2O_3 formation, perferryl ions weaken the O═O bond, acquire H^+ and attach one OH^- to sulfur sites on the pyrite surface, thereby oxidizing sulfur.

The intricate behavior of pyrite oxidation by H_2O_2 is due to (i) the high reactivity of oxidizing species produced during H_2O_2 disproportionation and catalytic reactions; (ii) competing oxidants with temperature-dependent oxidation efficiencies, and (iii) multiple reaction pathways for different temperature and surface conditions. Our results highlight the complexity of radical-driven reactions and reveal an intricate interplay among reactants and products, even for a simple geochemical system such as H_2O–pyrite–H_2O_2. In addition, these results underscore the need for further experiments to specifically examine oxygen isotope systematics during radiolysis of water coupled to oxidation of pyrite and other sulfide minerals.

In natural settings on Earth, additional important controls on supply and fate of radiolytic oxidants are mineral composition, mineral concentration, composition of dissolved species, mass transport parameters, and microbiology. Isotopic signatures acquired during oxidative processes in O_2-limited environments are an important diagnostic indicator of radiolytic production of oxidants. Additional evidence of radiolysis can be preserved in the form of unusual minerals such as the peroxide-containing mineral studite (Burns and Hughes, 2003) known from uranium ore bodies. Distinguishing among different mechanisms of pyrite oxidation is critical in assessing oxidative processes on Earth and other planetary bodies with ionizing solar radiation in surface settings and with radiolytic decomposition of water in subsurface environments.

ACKNOWLEDGMENTS

This research was supported by NASA Grant NNA 04CC03A through the NASA Astrobiology Institute. An NSF equipment grant to Juergen Schieber (EAR-0318769) provided funds for the purchase of the analytical SEM that was used for acquiring the images used in this report. We thank Peter Sauer for his intellectual and organizational support with oxygen isotope analysis. We are grateful to Jay LaVerne for many discussions regarding radiolysis. The manuscript greatly benefited from constructive criticism and helpful comments by Associate Editor David Cole, Don Rimstidt, and an anonymous reviewer.

REFERENCES

Abbot J. and Brown D. G. (1990) Kinetics of iron-catalyzed decomposition of hydrogen peroxide in alkaline solution. *Int. J. Chem. Kinet.* **22**, 963–964.

Aharon P. and Fu B. (2003) Sulfur and oxygen isotopes of coeval sulfate–sulfide in pore fluids of cold seep sediments with sharp redox gradients. *Chem. Geol.* **195**, 201–218.

Allen A. O. (1961) *The Radiation Chemistry of Water and Aqueous Solutions*. Van Nostrand, New York.

Alpers C. N., and Blowes D. W. (1994) Environmental geochemistry of sulfide oxidation. In *ACS Symp. Ser. 550*. American Chemical Society, Washington DC.

Amme M., Bors W., Michel C., Stettmaier K., Rasmussen G. and Betti M. (2005) Effects of Fe(II) and hydrogen peroxide interaction upon dissolving UO_2 under geologic repository conditions. *Environ. Sci. Technol.* **39**, 221–229.

Atreya S. K., Wong A., Renno N. O., Farrell W. M., Delory G. T., Sentman D. D., Cummer S. A., Marshall J. R., Rafkin C. R. and Catling D. C. (2006) Oxidant enhancement in Martian dust devils and storms: implications for life and habitability. *Astrobiology* **6**, 439–450.

Baird A. K., Toulmin, III, P., Clark B. C., Rose, Jr., H. J., Keil K., Christian R. P. and Gooding J. L. (1976) Mineralogic and petrologic implications of Viking geochemical results from Mars: interim report. *Science* **194**, 1288–1293.

Balbuena P. B., Calvo S. R., Lamas E. J., Salazar P. F. and Seminario J. M. (2006) Adsorption and dissociation of H_2O_2 on Pt and Pt alloy clusters and surfaces. *J. Phys. Chem. B* **110**, 17452–17459.

Banfield J. F. and Hengzhong Z. (2001) Nanoparticles in the environment. *Reviews in Mineralogy and Geochemistry* **44**, 1–58.

Banks D., Younger P. L., Arnesen R. T., Iversen E. R. and Banks S. B. (1997) Mine-water chemistry: the good, the bad, and the ugly. *Environ. Geol.* **32**, 157–173.

Barb W. G., Baxendale J. H., George P. and Hargrave K. R. (1949) Reactions of ferrous and ferric ions with hydrogen peroxide. *Nature* **163**, 692–694.

Bibring J. P., Langevin Y., Gendrin A., Gondet B., Poulet F., Berthé M., Soufflot A., Arvidson R., Mangold N., Mustard J. and Drossart P.and the OMEGA Team (2005) Mars surface diversity as revealed by the OMEGA/Mars Express observations. *Science* **307**, 1576–1581.

Bishop J. L., and Murad E. (1996) Schwertmannite in Mars? Spectroscopic analyses of schwertmannite, its relationship to other ferric minerals, and its possible presence in the surface material on Mars. In *Mineral Spectroscopy: A Tribute to Roger Burns* (eds. M. D. Dyar, C. McCammon, and M. W. Schaefer). Special Publication No. 5. Geochemical Society, London, pp. 337–358.

Böhlke J. K., Mroczkowski S. J. and Coplen T. B. (2003) Oxygen isotopes in nitrate: new reference materials for 18O:17O:16O measurements and observations on nitrate–water equilibration. *Rapid Commun Mass Spectr.* **17**, 1835–1846.

Bonnissel-Gissinger P., Alnot M., Ehrhardt J. J. and Behra P. (1998) Surface oxidation of pyrite as a function of pH. *Environ. Sci. Technol.* **32**, 2839–2845.

Borda M. J., Elsetinow A. R., Strongin D. R. and Schoonen M. A. (2003) A mechanism for the production of hydroxyl radical at surface defect sites on pyrite. *Geochim. Cosmochim. Acta* **67**, 935–939.

Borda M. J., Strongin D. R. and Schoonen M. A. (2004) A vibrational spectroscopic study of the oxidation of pyrite by molecular oxygen. *Geochim. Cosmochim. Acta* **68**, 1807–1813.

Böttcher M. E., Thamdrup V. and Vennemann T. W. (2001) Oxygen and sulfur isotope fractionation during anaerobic bacterial disproportionation of elemental sulfur. *Geochim. Cosmochim. Acta* **65**, 1601–1609.

Burns P. C. and Hughes K. A. (2003) Studtite, $[(UO_2)(O_2)(H_2O)_2](H_2O)_2$: the first structure of a peroxide mineral. *Am. Mineral.* **88**, 1165–1168.

Bray W. C. and Gorin M. H. (1932) Ferryl ion, a compound of tetravalent iron. *J. Am. Chem. Soc.* **54**, 2124–2125.

Buxton G. V. (1987). In *Radiation Chemistry: Principles and Applications* (eds. M. Farhataziz and A. J. Rodgers). VCH Publishers., New York, p. 321.

Buxton G. V., Greenstock C. L., Helman W. P. and Ross A. B. (1988) Critical-review of rate constants for reactions of hydrated electrons, hydrogen-atoms and hydroxyl radicals ($^{\cdot}OH/O^{-}$) in aqueous-solution. *J. Phys. Chem. Ref. Data* **17**, 513–886.

Cahill A. and Taube H. (1952) The use of heavy oxygen in the study of reactions of hydrogen peroxide. *J. Am. Chem. Soc.* **74**, 2312–2317.

Canfield D. E. (2001) Biochemistry of sulfur isotopes. In *Stable Isotope Geochemistry* (eds. J. V. Valley and D. R. Cole). Reviews in Mineralogy and Geochemistry 43, pp. 607–636.

Clark and 23 coauthors. (2005) Chemistry and mineralogy of outcrops at Meridiani Planum. *Earth Planet. Sci. Lett.* **240**, 73–94.

Chiba H. and Sakai H. (1985) Oxygen isotope exchange rate between dissolved sulfate and water at hydrothermal temperatures. *Geochim. Cosmochim. Acta* **49**, 993–1000.

Christensen P. R., and 26 coauthors. (2004) Mineralogy at Meridiani Planum from the Mini-TES experiment on the opportunity rover. *Science* **306**, 1733–1739.

Coplen T. B. (1996) New guidelines for reporting stable hydrogen, carbon, and oxygen isotope-ratio data. *Geochim. Cosmochim. Acta* **60**, 3359–3360.

Craig H. (1957) Isotopic standards for carbon and oxygen and correction factor for mass-spectrometric analysis of carbon dioxide. *Geochim. Cosmochim. Acta* **12**, 133–149.

Croiset E., Rice S. F. and Hanush R. G. (1997) Hydrogen peroxide decomposition in supercritical water. *AIChE J.* **43**, 2343.

DesMarais D. J. and Hayes J. M. (1976) Tube cracker for opening glass-sealed ampoules under vacuum. *Anal. Chem.* **48**, 1651–1652.

Dole M., Rudd D. P., Muchow G. R. and Comte C. (1952) Isotopic composition of oxygen in the catalytic decomposition of hydrogen peroxide. *J. Phys. Chem.* **20**, 961–968.

Dorfman L. M., and Adams, G. E. (1973) Reactivity of the hydroxyl radical in aqueous solutions. In *National Standard Reference System. Monograph NSRDS-NBS 46*. National Bureau of Standards, Washington, USA, pp. 1–59.

Druschel G. K., Hamers R. J., Luther G. W. and Banfield J. F. (2004) Kinetics and mechanism of trithionate and tetrathionate oxidation at low pH by hydroxyl radicals. *Aqueous. Geochem.* **9**, 145–164.

Dubessy J., Pagel M., Beny J. M., Christensen H., Hickel B., Kosztolanvi C. and Poty B. (1988) Radiolysis evidenced by H_2O_2 and H_2-bearing fluid inclusions in three uranium deposits. *Geochim. Cosmochim. Acta* **52**, 1155–1167.

Dunford H. B. (2002) Oxidation of iron(II)/(III) by H_2O_2: from aquo to enzyme. *Coord. Chem. R.* **233–234**, 311–318.

Dunn J. P., Stenger H. G. and Wachs I. E. (1999) Oxidation of SO_2 over supported metal oxide catalysts. *J. Catal.* **181**, 233–243.

Edwards K. J., Bond P. L., Gihring T. M. and Banfield J. F. (2000) An archaeal iron-oxidizing extreme Acidophile important in acid mine drainage. *Science* **287**, 1796–1799.

Elliot A. J., McCracken D. R., Buxton G. V. and Wood N. D. (1990) Estimation of rate constants for near-diffusion-controlled reactions in water at high temperatures. *J. Chem. Soc. Faraday Trans.* **86**, 1539–1547.

Elwood Madden M. E., Bodnar R. J. and Rimstidt J. D. (2004) Jarosite as an indicator of water limited chemical weathering on Mars. *Nature* **431**, 821–823.

Epstein S. and Mayeda T. (1953) Variation of ^{18}O contents of water from natural sources. *Geochim. Cosmochim. Acta* **4**, 213–224.

Evangelou V. P. (1995) *Pyrite Oxidation and Its Control*. CRC Press, Boca Raton, FL.

Evangelou V. P. and Zhang Y. L. (1995) A review: pyrite oxidation mechanisms and acid mine drainage prevention. *Crit. Rev. Environ. Sci. Technol.* **25**, 141–199.

Fayek M., Janeczek J. and Ewing P. C. (1997) Mineral chemistry and oxygen isotopic analyses of uraninite, pitchblende and uranium alteration minerals from the Cigar Lake deposit, Saskatchewan, Canada. *Appl. Geochem.* **12**, 549–565.

Garrels R. M. and Thompson M. E. (1960) Oxidation of pyrite by iron sulfate solutions. *Am. J. Sci.* **258A**, 57–67.

Garrett B. C. and 45 others. (2004) Role of water in electron-initiated processes and radical chemistry: issues and scientific advances. *Chem. Rev.* **105**, 355–390.

Gendrin A., Mangold N., Bibring J.-P., Langevin Y., Gondet B., Poulet F., Bonello G., Quantin C., Mustard J., Arvidson R. E. and LeMouélic S. (2005) Sulfates in martian layered terrains: the OMEGA/Mars Express view. *Science* **307**, 1587–1591.

Goldhaber M. B. (1983) Experimental study of metastable sulfur oxy-anion formation during pyrite oxidation at pH 6–9 and 30 °C. *Am. J. Sci.* **238**, 193–217.

González-Davila M., Santana-Casiano J. M. and Millero F. J. (2005) The oxidation of Fe(II) nanomolar with H_2O_2 in seawater. *Geochim. Cosmochim. Acta* **69**, 83–93.

Gray P. (1959) Chemistry of free radicals containing oxygen. II. Thermochemistry of the hydroxyl and hydroperoxy radicals. *Trans. Faraday Soc.* **55**, 408.

Grotzinger J. P. and 19 coauthors. (2005) Stratigraphy and sedimentology of a dry to wet eolian depositional environment, Burns formation, Meridiani Planum, Mars. *Earth Planet. Sci. Lett.* **240**, 11–72.

Haber F. and Weiss J. (1934) The catalytic decomposition of hydrogen peroxide by iron salts. *Proc. R. Soc.* **147**, 332–351.

Hiroki A. and LaVerne J. A. (2005) Decomposition of hydrogen peroxide at water–ceramic oxide interfaces. *J. Phys. Chem. B.* **109**, 3364–3370.

Jambor J. and Blowes D. W. (1994) Environmental geochemistry of sulfide mine wastes. *Mineral. Assoc. Can. Short Course*, 22.

Jambor J. L., Blowes D. W. and Ritchie A. I. M. (2003) Environmental aspects of mine wastes. *Min. Assoc. Can. Short Course Ser.* **31**, 430.

Kamei G. and Ohmoto H. (1999) The kinetics of reactions between pyrite and O_2-bearing water revealed from in situ monitoring of DO, Eh and pH in a closed system. *Geochim. Cosmochim. Acta* **64**, 2585–2601.

King D. W. (1998) Role of carbonate speciation on the oxidation rate of Fe(II) in aquatic systems. *Environ. Sci. Technol.* **32**, 2997–3003.

King D. W., Lounsbury H. A. and Millero F. J. (1995) Rates and mechanism of Fe(II) oxidation at nanomolar total iron concentration. *Environ. Sci. Technol.* **29**, 818–824.

Kminek G. and Bada J. L. (2006) The effect of ionizing radiation on the preservation of amino acids on Mars. *Earth Planet. Sci. Lett.* **245**, 1–55.

Koppenol W. H. and Liebman J. F. (1984) The oxidizing nature of the hydroxyl radical. A comparison with the ferryl ion (FeO^{2+}). *J. Phys. Chem.* **88**, 99–107.

Knoll A. H., and 12 coauthors. (2005) An astrobiological perspective on Meridiani Platum. *Earth Planet. Sci. Lett.* **240**, 179–189.

Kremer M. L. (1999) Mechanism of the Fenton reaction. Evidence for a new intermediate. *Phys. Chem. Chem. Phys.* **1**, 3595–3605.

Krouse H. R., Gould W. D., McCready R. G. L. and Rajan S. (1991) ^{18}O incorporation into sulfate during bacterial oxidation of sulfide minerals and the potential for oxygen isotope exchange between O_2, H_2O and oxidized sulfur intermediates. *Earth Planet. Sci. Lett.* **107**, 90–94.

Kwan W. and Voelker B. (2002) Decomposition of hydrogen peroxide and organic compounds in the presence of dissolved iron and ferrrihydrite. *Environ. Sci. Technol.* **36**, 1467–1472.

Lefticariu L., Pratt L. M. and Ripley E. M. (2006) Mineralogic and sulfur isotopic effects accompanying oxidation of pyrite in millimolar solutions of hydrogen peroxide at temperatures from 4 to 150 °C. *Geochim. Cosmochim. Acta* **70**, 4889–4905.

Lin L. H., Slater G. F., Sherwood Lollar B., Lacrampe-Couloume G. and Onstott T. C. (2005) The yield and isotopic composition of radiolytic H_2, a potential energy for the deep subsurface biosphere. *Geochim. Cosmochim. Acta* **69**, 893–903.

Lin L. H., Wang P. L., Rumble D., Lippmann-Pipke J., Boice E., Sherwood Lollar L. M., Pratt B., Brodie E. L., Hazen T. C., Andersen G. L., DeSantis T. Z., Moser D. P., Kershaw D. and Onstott T. C. (2006) Long-term sustainability of a high-energy, low-diversity crustal biome. *Science* **314**(5798), 479–482.

Lin S. S. and Gurol M. D. (1998) Catalytic decomposition of hydrogen peroxide on iron oxide: kinetics, mechanism, and implications. *Environ. Sci. Technol.* **32**, 1417–1423.

Liu J., Yu J. W. and Neretnieks I. (1996) Transport modeling in the natural analogue study of the Cigar Lake uranium deposit (Saskatchenwan, Canada). *J. Contam. Hydro.* **21**, 19–34.

Lloyd R. M. (1967) Oxygen-18 composition of oceanic sulfate. *Science* **156**, 1228–1231.

Lloyd R. M. (1968) Oxygen isotope behavior in the sulfate–water system. *J. Geophys. Res.* **73**, 6099–6110.

Lowson R. T. (1982) Aqueous pyrite oxidation by molecular oxygen. *Chem. Rev.* **82**, 461–497.

Luther, III, G. W. (1987) Pyrite oxidation and reduction: molecular orbital theory considerations. *Geochim. Cosmochim. Acta* **51**, 3193–3199.

McKibben M. A. and Barnes H. L. (1986) Oxidation of pyrite in low temperature acidic solutions: rate laws and surface textures. *Geochim. Cosmochim. Acta* **50**, 1509–1520.

McLennan S. M., and 31 coauthors. (2005) Provenance and diagenesis of the evaporite-bearing Burns Formation, Meridiani Planum, Mars. *Earth Planet. Sci. Lett.* **240**, 95–121.

Mizutani Y. and Rafter T. A. (1969a) Oxygen isotopic composition of sulphates, part 3: oxygen isotopic fractionation in the bisulphate ion–water system. *New Zeal. J. Sci.* **12**, 54–59.

Mizutani Y. and Rafter T. A. (1969b) Oxygen isotopic composition of sulphates, part 4: bacterial fractionation of oxygen isotopes in the reduction of sulphate and in the oxidation of sulphur. *New Zeal. J. Sci.* **12**, 60–68.

Mizutani Y. and Rafter T. A. (1973) Isotopic behavior of sulphate oxygen in the bacterial reduction of sulphate. *Geochem. J.* **6**, 183–191.

Moffett J. D. and Zika R. G. (1987) Reaction kinetics of hydrogen peroxide with copper and iron in seawater. *Environ. Sci. Technol.* **21**, 804–810.

Moses C. O., Nordstrom D. K., Herman J. S. and Mills A. L. (1987) Aqueous pyrite oxidation by dissolved oxygen and ferric iron. *Geochim. Cosmochim. Acta* **51**, 1561–1571.

Nordstrom D. K. and Alpers C. N. (1999) Geochemistry of acid mine waters. In *The Environmental Geochemistry of Mineral Deposits* (eds. G. S. Plumlee and M. J. Logsdon). Society of Economic Geologists, Littleton, CO, pp. 133–160.

Nordstrom D. K., Alpers C. N., Ptacek C. J. and Blowes D. W. (2000) Negative pH and extremely acidic mine waters from Iron Mountain, California. *Environ. Sci. Technol.* **34**, 254.

Pastina B. and LaVerne J. A. (2001) Effect of molecular hydrogen on hydrogen peroxide in water radiolysis. *J. Phys. Chem. A* **105**, 9316–9322.

Petrik N. G., Alexandrov A. B. and Vall A. I. (2001) Interfacial energy transfer during gamma radiolysis of water on the surface of ZrO_2 and some other oxides. *J. Phys. Chem. B* **105**, 5935–5944.

Reedy B. J., Beattie J. K. and Lowson R. T. (1991) A vibrational spectroscopic ^{18}O tracer study of pyrite oxidation. *Geochim. Cosmochim. Acta* **55**, 1609–1614.

Rimstidt J. D. and Vaughan D. J. (2003) Pyrite oxidation: a state-of the-art assessment of the reaction mechanism. *Geochim. Cosmochim. Acta* **67**, 873–880.

Rosso K. M., Becker U. and Hochella, Jr., M. F. (1999) The interaction of pyrite {100} surfaces with O2 and H_2O: fundamental oxidation mechanisms. *Am. Mineral.* **84**, 1549–1561.

Rush J. D. and Bielski B. H. J. (1985) Pulse radiolytic studies of the reactions of hydrodioxyl-superoxide with Fe(II)/Fe(III) ions. The reactivity of hydrodioxyl -superoxide with ferric ions and its implication on the occurrence of the Haber–Weiss reaction. *J. Phys. Chem.* **89**, 5062–5066.

Rye R. O., Bethke P. M. and Wasserman M. D. (1992) The stable isotope geochemistry of acid sulfate alteration. *Econ. Geol.* **87**, 225–262.

Sasaki K. (1994) Effect of grinding on the rate of pyrite oxidation by oxygen in acid solution. *Geochim. Cosmochim. Acta* **58**, 4649–4655.

Savary V. and Pagel M. (1997) The effects of water radiolysis on local redox conditions in the Oklo, Gabon, natural fission reactors 10 and 16. *Geochim. Cosmochim. Acta* **61**, 4479–4494.

Seal R. R. II. (2003) Stable-isotope geochemistry of mine waters and related solids. In: *Environmental Aspects of Mine Wastes* (eds. J. L. Jambor, D. W. Blowes, and A. I. M. Ritchie). Mineral. Assoc. Short Course 31, pp. 303–334.

Seal R. R. II, and Wandless, G. A. (1997) Stable isotope characteristics of waters draining massive sulfide deposits in the eastern United States. In *Proceedings of Fourth International Symposium on Environmental Geochemistry* (eds. R. B. Wanty, S. P. Marsh, and L. P. Gough). U.S. Geol. Surv. Open-File Report, pp. 97–496.

Singer P. C. and Stumm W. (1970) Acidic mine drainage: the rate determining step. *Science* **167**, 1121–1123.

Spinks J. W. T. and Woods R. J. (1990) *An Introduction to Radiation Chemistry*, third ed. Wiley, New York.

Squyres S. W. and 18 coauthors. (2004) In situ evidence for an ancient aqueous environment at Meridiani Planum, Mars. *Science* **306**, 1709–1714.

Schulze-Makuch D. and Irwin L. N. (2006) *Life in the Universe: Expectations and Constraints*. Springer, Berlin, 172 p.

Stefanic I. and LaVerne J. A. (2002) Temperature dependence of the hydrogen peroxide production in the radiolysis of water. *J. Phys. Chem. A* **106**, 447–452.

Stuglik Z. and Zagorski Z. P. (1981) Pulse-radiolysis of neutral iron(II) solutions-oxidation of ferrous-ions by OH radicals. *Radiat. Phys. Chem.* **17**, 229–233.

Taylor B. E., and Wheeler M. C. (1994) Sulfur and oxygen-isotope geochemistry of acid mine drainage in the western United States. In *Environmental Geochemistry of Sulfide Oxidation* (eds. C. N. Alpers, and D. W. Blowes). Am. Chem. Soc. Symp. Ser. 550, pp. 481–514.

Taylor B. E., Wheeler M. C. and Nordstrom D. K. (1984a) Isotope composition of sulfate in acid mine drainage as measure of bacterial oxidation. *Nature* **308**, 538–541.

Taylor B. E., Wheeler M. C. and Nordstrom D. K. (1984b) Stable isotope geochemistry of acid mine drainage: experimental oxidation of pyrite. *Geochim. Cosmochim. Acta* **48**, 2669–2678.

Todd E. C., Sherman D. M. and Purton J. A. (2003) Surface oxidation of pyrite under ambient atmospheric and aqueous (pH 2 to 10) conditions: electronic structure and mineralogy from X-ray absorption spectroscopy. *Geochim. Cosmochim. Acta* **67**, 881–893.

Toran L. and Harris R. (1989) Interpretation of sulfur and oxygen isotopes in biological and abiological sulfide oxidation. *Geochim. Cosmochim. Acta* **53**, 2341–2348.

Usher C. R., Paul C. W., Narayasamy J., Kubicki J. D., Sparks D. L., Strongin D. R. and Schoonen M. A. A. (2005) Mechanistic aspects of pyrite oxidation in an oxidizing gaseous environment: an in situ HATR-IR isotope study. *Environ. Sci. Technol.* **39**, 7576–7584.

Vaniman D. T., Bish D. L., Chipera S. J., Fialips C. I., Carey J. W. and Feldman W. C. (2004) Magnesium sulfate salts and the history of water on Mars. *Nature* **431**, 663–665.

van Everdingen R. O. and Krouse H. R. (1985) Isotope composition of sulfates generated by bacterial and abiological oxidation. *Nature* **315**, 395–396.

van Stempvoort D. R., and Krouse H. R. (1994) Controls on $\delta^{18}O$ in sulfate. In *Environmental Geochemistry of Sulfide Oxidation* (eds. C. N. Alpers, and D. W. Blowes). Am. Chem. Soc Symp. Ser. 550, pp. 446–480.

Vovk I. F. (1982) Radiolysis of underground waters as the mechanism of geochemical transformation of the energy of radioactive decay in sedimentary rocks. *Litho. Mineral. Res.* **16**, 328–334.

Vovk I. F. (1987) Radiolytic oxidation of sulphides and geochemical behavior of sulfur isotopes in uranium deposits. In *Studies on sulphur isotope variations in nature*. Vienna, Austria: International Atomic Energy Agency, pp. 85–103.

Warren C. G. (1972) Sulfur isotopes as a clue to the genetic geochemistry of roll-type uranium deposit. *Econ. Geol.* **67**, 759–767.

Weiss J. (1935) The catalytic decomposition of hydrogen peroxide on different metals. *Trans. Faraday Soc.* **31**, 1547–1557.

Weiss J. and Humphrey C. W. (1949) Reaction between hydrogen peroxide and iron salts. *Nature* **163**, 691–695.

Weiss J. (1952) Reaction mechanism of the enzymes catalase and peroxidase in the light of the theory of chain reactions. In *Advances in Catalysis*, Vol. 5 (eds. W. G. Frakernburg, E. K. Rideal and V. I. Komarewsky). Academic Press, New York, pp. 343–364.

Weinstein J. and Bielski B. H. J. (1979) Kinetics of the interaction of HO_2 and O_2-radicals with H_2O_2: the Haber–Weiss reaction. *J. Am. Chem. Soc.* **101**, 58–62.

Williamson M. A. and Rimstidt J. D. (1994) The kinetics and electrochemical rate determining step of aqueous pyrite oxidation. *Geochim. Cosmochim. Acta* **58**, 5443–5454.

Associate editor: David R. Cole